A positive feedback loop between ZEB2 and ACSL4 regulates lipid metabolism to promote breast cancer metastasis

Jiamin Lin1†, Pingping Zhang1†, Wei Liu2†, Guorong Liu1, Juan Zhang1, Min Yan3, Yuyou Duan4,5*, Na Yang1*

1 Department of Laboratory Medicine, Guangzhou First People's Hospital, South China University of Technology, Guangzhou, Guangdong, 510180, China.
2 Department of Breast Surgery, Guangzhou Red Cross Hospital, Guangzhou Red Cross Hospital of Jinan University, Guangzhou, Guangdong, 510220, China.
3 Sun Yat-sen University Cancer Center, State Key Laboratory of Oncology in South China, Collaborative Innovation Center of Cancer Medicine, Guangzhou, 510060, China.
4 Laboratory of Stem Cells and Translational Medicine, Institutes for Life Sciences and School of Medicine, South China University of Technology, Guangzhou, 510006, China.
5 Institute for Clinical Medicine, Guangzhou First People's Hospital, South China University of Technology, Guangzhou 510180, China.

†These authors contributed equally to this work.

*Correspondence to:
Na Yang, M.D., Ph.D.
Department of Laboratory Medicine
Guangzhou First People's Hospital
South China University of Technology
1 Panfu Road, Guangzhou 510180, P.R. China
E-mail: eyyangna@scut.edu.cn

Yuyou Duan, Ph.D.
Laboratory of Stem Cells and Translational Medicine
Institutes for Life Sciences, School of Medicine
South China University of Technology
No.382 Waihuan East Road, Suite 406
Higher Education Mega Center
Guangzhou 510006, P.R. China
E-mail: yuyouduan@scut.edu.cn

Min Yan, Ph.D

State Key Laboratory of Oncology in South China
Sun Yat-sen University Cancer Center
651 Dongfeng Road East, Guangzhou, 510060, P.R. China
Email: yanmin@sysucc.org.cn

Highlights

ZEB2 activates FAO through transcription of ACSL4
ACSL4 regulates lipid metabolism through FAO, promoting breast cancer metastasis
Targeting ZEB2-ACSL4 signaling axis inhibits breast cancer metastasis

Significance

We describe a novel positive feedback loop between ZEB2 and ACSL4 that results in enhanced cellular lipid storage and FA oxidation to drive breast cancer metastasis.

Running Title: A novel positive feedback loop between ZEB2 and ACSL4

Key Words: Lipid metabolism; Lipid droplet; cancer metastasis; EMT

Abstract

Lipid metabolism plays a critical role in cancer metastasis. However, the mechanisms through which metastatic genes regulate lipid metabolism remain unclear. Here, we describe a new oncogenic-metabolic feedback loop between the epithelial-mesenchymal transition (EMT) transcription factor ZEB2 and the key lipid enzyme ACSL4 (long-chain acyl-CoA synthetase 4), resulting in enhanced cellular lipid storage and fatty acid oxidation to drive breast cancer metastasis. Functionally, Depletion of ZEB2 or ACSL4 significantly reduced lipid droplets (LD) abundance and cell migration. ACSL4 overexpression rescued the invasive capabilities of the ZEB2 knockdown cells, suggesting that ACSL4 is crucial for ZEB2-mediated metastasis. Mechanistically, ZEB2 activated ACSL4 expression by directly binding to the ACSL4 promoter. ACSL4 binds to and stabilizes ZEB2 by reducing ZEB2 ubiquitination. Notably, ACSL4 not only promotes the intracellular lipogenesis and lipid droplet accumulation but also enhances fatty acid oxidation (FAO) and ATP production by upregulating the FAO rate-limiting enzyme CPT1A (carnitine palmitoyltransferase 1 isoform A). Finally, we demonstrated that ACSL4 knockdown significantly reduced metastatic lung nodes in vivo. In conclusion, we reveal a novel positive regulatory loop between ZEB2 and ACSL4, which promotes LD storage to meet the energy needs of breast cancer metastasis, and identify the ZEB2-ACSL4 signaling axis as an attractive therapeutic target for overcoming breast cancer metastasis.

Introduction

More than 90% of breast cancer-related deaths are due to metastasis(Fahad Ullah, 2019; Park et al., 2022). Current treatments, including endocrine therapy, chemotherapy, and radiation therapy, are ineffective in preventing breast cancer

metastasis and remain the greatest clinical challenge for breast cancer treatment(Barzaman et al., 2020). Cancer metastasis is associated with a process called epithelial-mesenchymal transition (EMT)(Luond et al., 2021; Mittal, 2018). EMT is a pre-metastatic state in which epithelial cells lose their tight junctions and convert to migratory mesenchymal cells(Dongre and Weinberg, 2019). It has become increasingly recognized that metabolic reprogramming during the EMT process contributes to metastasis and tumorigenesis(Kang et al., 2019; Sciacovelli and Frezza, 2017). Metastatic invasion is a highly energy-intensive process(Mosier et al., 2021). Emerging evidence suggests that lipid metabolic reprogramming plays a critical role in meeting the energy requirements of metastatic invasion(Bian et al., 2021; Cheng et al., 2018; Li et al., 2020; Snaebjornsson et al., 2020). Elucidating the mechanism by which reprogrammed lipid metabolism helps us exploit novel and attractive targets for metastatic therapeutic interventions.

Lipid metabolism includes a complex network of pathways that regulate fatty acid (FA) synthesis, storage, and degradation(Maan et al., 2018). For lipid anabolism, FA are stored in a dynamic organelle called a lipid droplet, which is composed of a monolayer of phospholipids that covers a hydrophobic core containing neutral lipids, such as triacylglycerol (TAG) and cholesteryl esters (CE)(Cruz et al., 2020). Lipid droplets (LD) accumulation is associated with aggressiveness in many cancer types(Antunes et al., 2022), including breast(Zembroski et al., 2021), brain(Taib et al., 2019), liver(Niu et al., 2021), lung(Jin and Yuan, 2020), and prostate(Huang et al., 2012; Roman et al., 2020). Indeed, the aggregation of FA in LD is considered a priming state to prepare for metastasis(Petan, 2020; Rozeveld et al., 2020; Senga et al., 2018). In the case of need, FA can be released and oxidized for energy support. For example, it has been reported that fatty acids stored in lipid droplets were a crucial resource in fueling the metastatic process in pancreatic cancer (Rozeveld et al., 2020). Additionally, previous studies have suggested that metastatic triple-negative breast cancer (TNBC) depends on fatty acid oxidation (FAO) to produce high ATP levels (Camarda et al., 2016; Wright et al., 2017). Although lipid metabolism is crucial for cancer metastasis, the signalling pathway that regulates lipid metabolic reprogramming during breast cancer metastasis remains unclear.

Dysregulation of lipid metabolic enzymes has been documented in cancer metastasis(Luo et al., 2017). Long-chain fatty acyl synthetase (ACSL) 4 belongs to the long-chain acyl-CoA synthetase ligase enzyme family (Quan et al., 2021; Rossi Sebastiano and Konstantinidou, 2019). ACSL4 catalyses the conversion of long-chain FAs to acyl-CoAs, a necessary step for free long-chain FAs to enter the next metabolic pathway(Kuwata and Hara, 2019). The increased expression and activity of ACSL4 have been observed in many cancer types and are well-known biomarkers of ferroptosis(Doll et al., 2017). Although it has been reported that ACSL4 is a tumor suppressor that activates ferroptosis, many studies have suggested that ACSL4 is an oncogene that contributes to tumor progression. For example, ACSL4 promotes Hepatocellular carcinoma (HCC) cell proliferation and metastasis via lipogenesis and

lipid droplet accumulation(Chen et al., 2020; Niu et al., 2021). In prostate cancer, ACSL4 promotes cell growth, invasion, and hormonal resistance(Wu et al., 2015). The function of ACSL4 in breast cancer has been implicated in hormone therapy resistance involving the regulation of energy-dependent transporter expression(Orlando et al., 2019). However, regulation of lipid metabolism by ACSL4 during breast cancer invasion remains unclear.

In the present study, we demonstrate a novel positive feedback loop between the EMT transcription factor ZEB2 and the essential lipid metabolic enzyme ACSL4, resulting in enhanced cellular lipid droplet accumulation and fatty acid oxidation to drive breast cancer metastasis. Mechanistically, ZEB2 activates ACSL4 expression by directly binding to the ACSL4 promoter. ACSL4 stabilizes and upregulates ZEB2 via transcriptional and post-transcriptional mechanisms. In addition, we also provide evidence that overexpression of ZEB2 or ACSL4 is associated with worse prognosis in advanced breast cancer. Our findings provide insights into lipid metabolic mechanisms during the EMT process and reveal a novel oncogenic-metabolic pathway critical for breast cancer EMT and metastasis.

Materials and Methods

Breast cancer cell lines and clinical specimens

Breast cancer cell lines MCF-7, MDA-MB-231, and BT549 were purchased from the American Type Culture Collection (ATCC, Beijing Zhongyuan Ltd., Beijing, China). Paclitaxel-resistant and epirubicin-resistant cell lines have been reported previously (Yang et al., 2017; Zheng et al., 2014). All cell lines were maintained in Dulbecco's modified Eagle's medium (GIBCO) supplemented with 10% (v/v) FBS (BI, Biological Industries) and 1% (v/v) Pen/Strep (GIBCO) and incubated in a humidified atmosphere of 5% CO_2 at 37 °C.

Primary breast cancer and adjacent normal tissues were collected from the volunteers at Guangzhou First People’s Hospital, Guangdong, China. This study was approved by the Ethics Committee of the Guangzhou First People’s Hospital (approval no. K2021-201-01). Fourteen patients were enrolled in this study. The specimens were then subjected to western blotting and immunohistochemistry (IHC) assays.

Plasmid construction and cell transfection

The PLKO.1-TRC-LUC lentivirus vector containing shRNA (shACSL4-1 and shACSL4-2) and the control vector were purchased from WZ Biosciences. The virus package plasmids psPAX2 and pMD2.G were purchased from Addgene. To produce the lentivirus, the shRNA vector and package plasmids were co-transfected into 293T cells using polyethyleneimine (Polysciene). After 48 hours or 72 hours, supernatants were harvested and passed through 0.45 um filters to collect the virus and stored at -80 °C until further use. MDA-MB-231 cells were transfected with a viral solution containing 8ug/ml polybrene (Hanbio Biotechnology). 48 hours after transfection, the

169 virus was removed from the culture and fresh medium was added. The cells were
170 subsequently selected using 2 mg/mL puromycin to obtain a stable cell line. MCF-7
171 cells were transfected with HBLV-h-ACSL4-3xflag-ZsGreen-PURO or control lentiviral
172 plasmid. The plasmids were purchased from Hanbio Biotechnology.
173
174 For the siRNA assay, 5 nM negative control siRNA or ACSL4 and ZEB2 siRNA
175 (GenePharma) were transfected into MDA-MB-231 or paclitaxel-resistant cells using
176 Lipofectamine 3000 (Invitrogen) according to the manufacturer's instructions. Six
177 hours after transfection, the medium was replaced with fresh growth medium and the
178 cells were harvested after 24-48 hours for qPCR or western blot analysis. The siRNA
179 sequences are listed in Supplementary Table S1.

180

181 **Western blot analysis**
182 For western blotting, cells were lysed in WIP buffer (Beyotime) containing protease
183 and phosphatase inhibitors. Protein levels were quantified by BCA assay (Beyotime),
184 and equal amounts were separated using 10% SDS-PAGE electrophoresis and
185 transferred onto a 0.22 μm PVDF membrane for probing. After blocking for 1 hour in 5%
186 non-fat milk diluted in TBST, the membrane was incubated with various primary
187 antibodies at 4°C overnight. The following primary antibodies were used: ACSL4
188 (ab155282, Abcam), ZEB2 (sc-271984, Santa Cruz), E-cadherin (3195S, CST),
189 N-cadherin (610921, BD Biosciences), vimentin (D21H3, 5741T, CST), CPT1A
190 (ab220789, Abcam), GAPDH (10494-1-AP, Protein Tech), Myc-Tag (71D10, 2278T,
191 CST), and HA-Tag (C29F4, 3724T, CST). Next, secondary antibodies were added and
192 the proteins were detected using an ECL kit (Millipore). Immunoreactive signals were
193 visualized using the GE Amersham Imager 600 chemiluminescence system.

194

195 **Migration and invasion assay**
196 A wound healing assay was performed to examine the migratory ability of the cells.
197 Briefly, cells were seeded in 6-well plates at a density of 4×10^5 cells per well in a
198 complete medium at 37 °C. Until cells reached 80-90% density, a sterile plastic tip
199 was used to create a wound line across the surface of the plates. The suspended
200 cells were discarded. After The cells were cultured in reduced serum DMEM medium
201 in a 5% CO_2 incubator at 37 °C for 48 hours. Images were obtained using a
202 phase-contrast microscope. Each assay was performed in triplicates.
203
204 The cell invasion capacity was measured using Matrigel-coated Transwell chambers
205 (8.0 μm; Corning Inc.). Briefly, cells were suspended in 200 μL serum-free medium
206 and seeded in the upper chamber of a Transwell. The lower chamber of the Transwell
207 was filled with medium containing 10% FBS-containing medium. The Transwell
208 chambers were then incubated at 37 °C. After culturing for 24 hours, the Transwell
209 holes were penetrated with 4% paraformaldehyde for 20 minutes and then stained
210 with 0.1% crystal violet solution for 15 minutes. Invading cells were imaged and

counted in five random fields.

Immunofluorescence (IF) and Immunohistochemistry (IHC) assays

For the immunofluorescence assay, cells were seeded on confocal dishes, washed in PBS three times, and fixed in 4% paraformaldehyde for 15 minutes at room temperature. The cells were blocked with 10% goat serum (AR0009, BOSTER) for 1 h at room temperature and washed three times. The cells were then incubated with the primary antibodies for 1 hour at room temperature. Subsequently, the cells were rinsed thrice with PBS and incubated with secondary antibodies for 1 hour at room temperature.

For BODIPY 493/503 staining, cells were fixed in 4% PFA for 15 minutes and washed twice with PBS. The cells were then incubated with BODIPY 493/503 (1:2500 in PBS, GLPBIO) for 15 minutes at room temperature. DAPI was used to stain the nuclei. Images were acquired by confocal microscopy (Ni-E-A1, Nikon, 40x) and analyzed using NIS Elements Viewer software and ImageJ.

For immunohistochemistry (IHC) assay, paraffin-embedded tissue slides were dewaxed with xylene and rehydrated using a graded series of alcohols. This was followed by antigen retrieval and blocking with 5% BSA for 60 minutes. After that, Tissue slices were incubated with primary antibodies against ACSL4, ZEB2, Vimentin or ERα at 4 °C overnight in a humidified container and then detected with the SP Rabbit&Mouse HRP Kit (CWBIO). Images were acquired using a digital pathology scanning system (Aperio CS2).

Metabolic analysis

For the oxygen consumption rate (OCR) assay, the XF long-chain fatty acid oxidation (LCFA) stress test Kit (103672-100) and Seahorse XF96 Analyzer were used to investigate the long-chain fatty acid OCR and extracellular acidification rate (ECAR) according to the manufacturer's protocol.

ATP levels were determined using an ATP Assay Kit (S0026, Beyotime) according to the manufacturer's protocol. ATP levels were calculated using luminescence signals and were normalized to protein concentrations. Glycolytic activity was determined using a Glycolysis Cell-Based Assay Kit (600450, Cayman Chemical), according to the manufacturer's protocol.

Untargeted lipidomics and proteomics

Cell Lipids were extracted in a chloroform-methanol mixed solution (2:1, -20 °C). The extracted cell lysates were immersed in liquid nitrogen and frozen for 5 minutes. The extracted cell lysates were placed in a 2 ml adapter, and the above steps were

252 repeated twice. Samples were then centrifuged to pellet the proteins (5 minutes,
253 12000 rpm), and the supernatant was stored for analysis in a vacuum centrifugal
254 concentrator. The sample was dissolved in 200 μl isopropanol, filtered through a 0.22
255 μm membrane, and detected by Liquid Chromatography-Mass Spectrometry (LC-MS).
256 The lipidomics data were analyzed using LipidSearch software (version 4.0). The
257 software identified intact lipid molecules based on their molecular weight and
258 fragmentation pattern using an internal library of predicted fragment ions per lipid
259 class. The spectra were then aligned based on retention time and the MS1 peak
260 areas were quantified across the sample conditions. Excel 2010 was used to calculate
261 intensity, and the R program (version 3.2.5) was used for data manipulation and
262 statistical analyses, including unsupervised hierarchical clustering and heatmap
263 visualization.

264

265 **Quantitative Real-time PCR**

266 Total RNA was isolated using the TRIzol reagent (Invitrogen), and cDNAs was
267 synthesized from total RNA using the PrimeScript™ RT Master Mix (Perfect Real
268 Time, Takara). Quantitative real-time PCR was performed in triplicate using PowerUp
269 SYBR Green (Thermo Fisher Scientific). The relative gene expression was measured
270 using the $2^{-\Delta\Delta Ct}$ method. All primers used are listed in Supplementary Table S2.

271

272 **Luciferase reporter assays**

273 For Luciferase assays, the 2000bp ACSL4 promoter vector containing luciferase was
274 purchased from WZ Biosciences Inc. The -287bp, -965bp, -1038bp, and -1116bp
275 regions of the ACSL4 promoter were cloned by PCR amplification using primers
276 containing restriction sites MIII and Hind III. The nucleotide sequences of primers
277 used are listed in Supplementary Table S3. 293T cells were transfected with 1ug of
278 the-287bp, -965bp, -1038bp, -1116bp or 2000bp ACSL4 promoter luciferase reporter
279 and an empty vector for 24 hours. After transfection, the cells were harvested and
280 analyzed using Bright-Glo reagent (Promega) according to the manufacturer's
281 instructions.

282

283 **Chromatin immunoprecipitation (ChIP) assay**

284 ChIP assays were performed using a ChIP assay kit (Cat.p2078, Beyotime
285 Biotechnology). Briefly, MDA-MB-231 cells were grown to 90% confluence and
286 crosslinking was performed with 1% formaldehyde for 10 minutes. Mouse anti-ZEB2
287 antibody or mouse IgG was used to immunoprecipitate the DNA-containing
288 complexes. After the DNA purification (Cat. D0033; Beyotime Biotechnology), PCR,
289 and Q-PCR were performed to detect the ZEB2-binding site in the ACSL4 promoter
290 region. The primer sequences are listed in Supplementary Table S4.

291

292 **Co-immunoprecipitation (Co-IP) assay and Ubiquitination assay**

293 For co-IP assays, HEK293T cells were co-transfected with ACSL4-FLAG and
294 ZEB2-MYC plasmids. 48 hours after transfection, cells were lysed in WIP buffer
295 (Beyotime) containing a protease inhibitor and phosphatase inhibitors for 30 minutes
296 at 4 °C followed by centrifugation. The supernatants were immunoprecipitated with
297 the indicated antibodies overnight at 4 °C, followed by incubation with protein A/G
298 beads for 1 hour at 4 °C. After incubation, the beads were washed with WIP buffer and
299 boiled in a 2×loading buffer. Protein samples were analyzed by western blotting.

300

301 For the ubiquitination assay, HEK293T cells were transfected with HA-Ubi plasmid,
302 ACSL4-FLAG plasmid, and ZEB2-MYC or vector plasmid. 48 hours after transfection,
303 the cells were treated with 20 μM MG-132 for 6 hours to block the proteasomal
304 degradation of ZEB2 before being lysed with WIP lysis buffer (Beyotime). Equal
305 amounts of protein lysates were immunoprecipitated with anti-MYC beads and
306 subjected to SDS-PAGE, followed by blotting with anti-HA (ubiquitin) to visualize
307 polyubiquitinated ZEB2 protein bends.

308

309 **In vivo experiments**

310 The Ethics Committee approved the animal experiments for Animal Experiments of
311 the South China University of Technology. All NSG mice were purchased from the
312 Medical Laboratory Animal Center of Guangdong Province, China. Six female NSG
313 mice aged 6-8 weeks were used in each group for the primary tumor growth and
314 spontaneous lung metastasis experiments. A total of 2×10^6 vector control or
315 shACSL4 cells were mixed 1:1 by volume with Matrigel (BD Biosciences). Each
316 mouse was injected orthotopically into both the flanks. Xenograft tumor growth was
317 measured and tumor volume was calculated as follows: volume=(length×width^2)/2. At
318 the experimental endpoint, mice were intraperitoneally injected with 150 mg/kg
319 D-luciferin and imaged for 2 minutes using a live imager. The xenograft tumor and
320 lung samples were removed and fixed to count the metastatic lung nodules.

321

322 **Statistical analysis**

323 The results are reported as the mean ± standard deviation (SD) or mean ± standard
324 error of the mean (SEM), as indicated in the figure legend. Statistical comparisons
325 were performed using an unpaired two-sided Student's t-test and considered
326 significant if * $P<0.05$, ** $P<0.01$, *** $P<0.001$, and **** $P<0.0001$. Statistical
327 comparisons for the LM2 lung metastasis assay were performed using the Mann–
328 Whitney U test. All experiments with representative images, including western blotting
329 and immunofluorescence, were repeated at least twice, and representative images
330 are shown.

Results

ZEB2 and ACSL4 are overexpressed and correlated in highly invasive breast cancer cells

To explore the molecular mechanism of highly invasive breast cancer, we performed RNA sequencing analysis of wild-type and two drug-resistant luminal breast cancer cell lines. Significant changes in 6155 genes ($P < 0.05$). Notably, EMT and stemness genes such as ZEB2, SNAIL, TWIST, TRAIL, Gli2, WNT, and AKT3, which are overexpressed in basal-like breast cancer (BLBC), were significantly upregulated in drug-resistant cells (Supplementary Fig. S1A). In contrast, differentiated genes such as FOXA1, ERα, E-cadherin, and GATA3, which are highly expressed in the luminal subtype, were significantly downregulated (Supplementary Fig. S1B), suggesting that drug-resistant cells underwent EMT and became stem-like cells. We noticed that the rate-limiting enzymes of fatty acid metabolism, long-chain fatty acyl synthetase 4 (ACSL4), and EMT transcription factor ZEB2 were among the top 200 upregulated (>1.5-fold) genes (Fig. 1A). To verify these findings in the clinical sample, we analyzed ZEB2 and ACSL4 expression in TCGA database and found that ACSL4 expression was positively correlated with ZEB2 expression (Fig. 1B, $r=0.7657$, $p<0.001$) and inversely correlated with ERα expression (Fig. 1C, $r=-0.3312$, $p<0.001$). Using the Kaplan–Meier plotter database, we compared the post-progression survival (PPS) between ACSL4 or ZEB2 high- and low-expression breast cancer patients. We found that patients with higher ACSL4 or ZEB2 expression had worse prognosis than patients with advanced breast cancer (Fig. 1D and 1E). It is worth noticing that there is no difference in the overall survival between ACSL4 or ZEB2 high and low-expression breast cancer patients (supplementary Fig. S2).

To confirm this correlation, we performed western blot analysis and found that Basal-like and Taxol-resistant cell lines, which lack ERα expression, showed high expression of ZEB2 and ACSL4, whereas low or no ZEB2 and ACSL4 expression was detected in luminal subtype cell lines (Fig. 1F). Consistently, tissue samples from nine breast cancer patients had similar expression patterns, with ZEB2 and ACSL4 being relatively highly expressed in ER-negative patient samples (patients 6, 7, 8, and 9) (Fig. 1G and 1H). The immunohistochemistry staining assay, shown in Fig. 1I, also confirmed that ACSL4 and ZEB2 expression was elevated in ERα-negative breast carcinomas compared with ERα-positive breast carcinomas. Taken together, these results indicate that ACSL4 and ZEB2 are correlated and overexpressed in highly invasive breast cancers.

Overexpression of ACSL4 contributes to ZEB2-mediated breast cancer invasion.

Because ACSL4 is overexpressed in highly invasive breast cancer cells, we

hypothesized that ACSL4 is essential for driving breast cancer migration and invasion. We then established a stable ACSL4 overexpressed MCF7 cell line, which was less aggressive than the basal-like breast cancer cells. The overexpression of ACSL4 significantly enhanced the metastatic and invasive capacities of MCF7 cells (Fig. 2A and 2B). Conversely, ACSL4 knockdown by shRNA significantly reduced the metastatic and invasive capacity of MDA-MB-231 cells compared to that of the control cells (Fig. 2C and 2D). We also observed that the metastatic and invasive abilities of MDA-MB-231 cells were significantly reduced in ZEB2 knockdown cells (Supplementary Fig. S3). To investigate the downstream genes regulated by ACSL4, we performed RNA sequencing analysis and identified that the tight junction and focal adhesion pathways were among the most upregulated pathways in ACSL4 knockdown cells compared to control cells (Fig. 2E). To verify the RNA-seq results, we examined the expression of adhesion-related genes by immunoblotting and found that after silencing of ACSL4 and ZEB2, the luminal epithelial marker E-cadherin was increased, whereas the mesenchymal markers vimentin and N-cadherin were decreased (Fig. 2F). These results confirm the essential role of ACSL4 in breast cancer invasion and migration.

We hypothesized that the ZEB2-ACSL4 axis played a crucial role in metastatic ability. To examine whether ACSL4 was required for ZEB2-mediated breast cancer invasion and migration, ACSL4 was overexpressed in ZEB2-silencing cells (Fig. 2G). As expected, overexpression of ACSL4 significantly restored the invasive and metastatic capacities of ZEB2 knockdown cells by 35.1% and 32.4%, respectively (Fig. 2H and 2I), indicating that ACSL4 is essential for ZEB2-mediated breast cancer invasion and migration.

ACSL4 and ZEB2 promote Lipid droplet production and lipogenesis

ACSL4 is a member of the long-chain acyl-CoA synthetase family, which catalyzes the conversion of long-chain fatty acids into their active forms. However, the mechanism by which ACSL4 regulates lipid metabolism in breast cancer remains unclear. A previous study revealed that ACSL4 promotes lipid droplets (LD) accumulation in hepatocellular carcinoma (HCC)(Niu et al., 2021). Thus, we measured the basal LD content of breast cancer cells, including MCF-7, MDA-MB-231, and Taxol-resistant MCF-7 cells. The basal number and size of lipid droplets were significantly larger in MDA-MB-231 and Taxol-resistant MCF-7 cells, both of which are highly invasive breast cancer cell lines (Fig. 3A). Fluorescence microscopy revealed that ACSL4 co-localized with LD in MDA-MB-231 cells (Supplementary Fig. S4). Notably, ACSL4 knockdown reduced cytoplasmic LD abundance and LD-containing cells in MDA-MB-231 cells (Fig. 3B). Consistently, cytoplasmic LD abundance and LD-containing cells was significantly reduced in ZEB2-depleted cells (Fig. 3C).

Lipid droplets are phospholipid monolayers containing a hydrophobic core comprising triacylglycerols (TG) and cholesterol esters (CE). As ACSL4 promotes intracellular LD

accumulation in breast cancer cells, we investigated the effect of ACSL4 on the lipid composition of breast cancer cells. Untargeted Lipidomic analyses revealed that ACSL4 knockdown breast cancer cells had a reduced ability to incorporate long-strain monounsaturated (18:1, 17:1, 22:1, 24:1, 26:1) and saturated FA (16:0, 18:0, 24:0, 26:0) into triacylglycerol and phospholipids (PL), indicating that ACSL4 promotes the incorporation of long-chain monounsaturated and saturated fatty acids into triacylglycerol and phospholipids in these cells (Fig. 3D and 3E). Moreover, all these lipids, including triacylglycerol, phospholipids, and cholesterol esters, decreased the incorporation of several polyunsaturated FA, such as 22:6, 20:4, 22:4, and 22:5, in ACSL4 depleted cells as reported previously (Fig. 3D and Supplementary Fig. S5A)(Doll et al., 2017). Consistently, the total amount of different lipid species, as shown in Supplementary Fig. S5B, were significantly decreased after ACSL4 knockdown. All together, these results suggest that ACSL4 directs the long train of free fatty acids into lipid anabolism to form different lipid species in the LD or other cellular membranes.

Exogenous fatty acid promotes LD accumulation and fuel cell invasion

A previous study reported that some tumors tended to increase their intake of extracellular fatty acids to promote migration(Rozeveld et al., 2020). As we observed that depletion of ACSL4 greatly reduced cytoplasmic LD abundance and invasive potential in basal-like breast cancer cells, we hypothesized that LD accumulation is an important step prior to breast cancer invasion. To verify our hypothesis, we examined whether exogenous fatty acids contributed to LD accumulation and the invasive ability of breast cancer cells. Exogenous oleic acid (OA) was added to the cell culture medium. Treatment with oleic acid dramatically enhanced LD abundance in the cells (Fig. 4A and 4B), indicating that breast cancer cells tend to store lipids in LD for energy reserves. Next, we assessed the effects of exogenous oleic acid treatment on cell migration. Transwell and Wound healing assays revealed that oleic acid-treated cells exhibited significantly enhanced invasive and metastatic capacities compared with control cells (Fig. 4C and 4D).

Previous study reported that LD undergo lipolysis during the process of migration in pancreatic cancer(Rozeveld et al., 2020). We reasoned that breast cancer cells utilize stored lipids during migration to fuel metastasis. Lipid droplet content was analyzed using fluorescence microscopy after cell migration. Interestingly, we observed significantly reduced LD in cells on the lower side of the transwell chamber, suggesting that lipids stored in LD were utilized and degraded during cell migration (Fig. 4E). Taken together, these results suggest that lipids stored in lipid droplets are a crucial resource to fuel the process of breast cancer invasion and migration.

ACSL4 and ZEB2 stimulate long-chain fatty acid oxidation and ATP generation in BLBC Cells

To explore the mechanisms by which ACSL4 regulates lipid metabolism, we performed RNA sequencing to investigate downstream pathways and genes regulated by ACSL4. KEGG enrichment analysis revealed that the FAO pathway was among the top 20 regulated pathways (Fig. 5A). ACSL4 knockdown reduced the expression of genes involved in the FAO pathways (Fig. 5B). Importantly, we observed that the FAO rate-limiting enzyme CPT1A was significantly reduced in ACSL4 knockdown cells (Fig. 5B). Reverse transcription PCR confirmed that deletion of ACSL4 significantly reduced the expression of CPT1A, but did not affect the expression of CPT1B and CPT1C (Fig. 5C). Consistently, ACSL4 silencing reduced CPT1A protein expression (supplementary Fig. S6A). In addition, levels of other lipid metabolic enzymes, such as ATGL, FASN, and SREBP2, were significantly decreased after ACSL4 knockdown (Supplementary Fig. S6B). As ACSL4 knockdown decreased CPT1A expression, we reasoned that ACSL4 might stimulate fatty acid oxidation in highly invasive breast cancer. Oxygen consumption rate (OCR) was calculated in ACSL4 or ZEB2 silencing and control cells. We observed that the OCR rate derived from long-chain fatty acids was significantly reduced in ACSL4 or ZEB2 silencing cells (Fig. 5D and 5E), suggesting the metabolic advantage of increased long-chain fatty acid oxidation and oxidative phosphorylation (OXPHOS).

Since OXPHOS is accompanied by increased ATP generation, we measured ATP levels and found that ACSL4 or ZEB2 knockout cells had significantly reduced ATP generation compared to control cells (Fig. 5F and 5G). To exclude OXPHOS derived from the aerobic glycolysis pathway, we measured lactate production and found no significant difference in lactate production between ACSL4 or ZEB2 knockdown and control cells, suggesting that glucose metabolism is not involved in ACSL4 or ZEB2 mediated metabolic process (Fig. 5H and 5I). These results indicated that ACSL4 upregulates CPT1A to stimulate fatty acid oxidation and ATP generation in BLBC Cells.

ZEB2 transcriptionally activates the expression of ACSL4

ZEB2 is a crucial transcription factor involved in EMT. Because ZEB2 and ACSL4 were highly correlated in the clinical samples in TCGA database, we investigated whether ACSL4 is a direct downstream target of ZEB2. Silencing of ZEB2 by siRNA in MDA-MB-231 cells significantly reduced ACSL4 mRNA levels and protein expression in MDA-MB-231 cells (Fig. 6A and 6 B). We found that the ACSL4 promoter contained four canonical ZEB2-binding E-boxes (CAGGT/CACCT) located at -287, -965, -1038, and -1116 of the ACSL4 promoter, respectively (Fig. 6C). Therefore, we cloned five segments of the ACSL4 promoter and a control segment to generate promoter-luciferase constructs, based on the location of these E-boxes (Fig. 6C). ZEB2 overexpression significantly enhanced the luciferase activity of all five E-box-containing segments of the ACSL4 promoter, whereas no significant change was observed in the control segment (Fig. 6D). To examine whether ZEB2 directly binds to the ACSL4 promoter, we performed chromatin immunoprecipitation (ChIP)

using four sets of primers (Fig. 6E). Primer set 1, which covered segment 1, consistently exhibited apparent ZEB2 binding (Fig. 6F and 6G). However, no binding was detectable using the other three sets (Fig. 6F), indicating that ZEB2 binds to the E-Box located at nucleotides -184 to -295 of the ACSL4 promoter.

Since the -287 E-box exhibited apparent ZEB2 binding, we generated mutants of the -287 E-box promoter-luciferase construct. The Luciferase Reporter Assay revealed that ACSL4 promoter activity was almost entirely abolished by the mutations (Fig. 6H), suggesting that this promoter region is essential for ZEB2-mediated ACSL4 promoter activation. Taken together, these data suggest that ZEB2 directly binds to the ACSL4 promoter to activate its mRNA expression.

ACSL4 reduces ZEB2 mRNA expression and protein stabilization

We hypothesized that ACSL4 regulates the expression of ZEB2. We then performed quantitative PCR and immunoblotting and observed that both ZEB2 mRNA and protein levels were reduced after the depletion of ACSL4 in the two BCSC cell lines (Fig. 7A and 7B). A previous study has reported that ACSL4 regulates c-Myc protein stability in HCC. We reasoned that ACSL4 might in turn regulate the stability of ZEB2. Therefore, we performed a ubiquitination assay to investigate whether ACSL4 regulates ZEB2 protein stability via ubiquitination. HEK293T cells were co-transfected with HA-ubiquitin and myc-ZEB2 expression vectors along with either an empty vector or an ACSL4 overexpression vector. As shown in Fig. 7C, the expression of ACSL4 caused a significant decrease in the ubiquitination of ZEB2, suggesting that ACSL4 attenuated the ubiquitin proteolysis of ZEB2. Notably, co-IP assays revealed a specific interaction between ACSL4 and ZEB2 proteins, supporting the notion that ZEB2 and ACSL4 are present in a protein complex (Fig. 7D). To further confirm the role of ACSL4 in the regulation of ZEB2 proteolysis, cycloheximide was added to the cell medium to block the synthesis of new proteins. Interestingly, endogenous ZEB2 protein levels were almost completely suppressed in ACSL4 knockdown cells from 0h to 8h time points (Fig. 7E and 7F). This phenomenon could be explained by the fact that ZEB2 mRNA levels were significantly suppressed by the ACSL4 knockdown. Conversely, ZEB2 protein maintained a relatively steady level at 6 hours in ACSL4 overexpressing cells compared with control cells that undergone obvious ZEB2 proteolysis at 4 hours after adding CHX, indicating an increased ZEB2 protein stability in ACSL4 overexpressing cells (Fig. 7G and 7H). Taken together, these results indicate that ACSL4 not only stabilizes the ZEB2 protein by attenuating its ubiquitination but also upregulates ZEB2 mRNA expression. Therefore, ACSL4 regulates ZEB2 through both transcriptional and post-transcriptional mechanisms.

ACSL4 knockdown inhibits lung metastasis of BLBC in the animal model

To further validate our in vitro findings, we examined the effect of ACSL4 on lung metastasis of breast cancer cells in an animal model. Depletion of ACSL4 resulted in a significant reduction in tumor growth and lung colonization of highly metastatic

MDA-MB-231 cells (Fig. 8A). In contrast, the control group showed significantly more lung metastatic nodules (Fig. 8B) and rapid tumor growth (Fig. 8C and 8D). Immunohistochemistry confirmed a striking downregulation of ACSL4, accompanied by ZEB2 and vimentin, compared to those in the control group (Fig. 8E).

To further validate the role of LD in ACSL4 high-expression cells, we examined LD content in frozen sections of the two groups. Consistent with the in vitro results, there was an obvious reduction in LD accumulation in the ACSL4 depletion tissue compared to that in control tissue (Fig. 8F). Taken together, these data suggest that ACSL4 promotes the lung metastasis of breast cancer cells in vivo.

Discussion

The rewiring of metabolic pathways during EMT has only recently been recognized. In addition to glycolysis, dysregulated lipid metabolism has been shown to contribute to cancer invasion and metastasis(Corbet et al., 2020; Soukupova et al., 2021). Many EMT-driving factors have been found to reprogram the lipid metabolic pathways by regulating metabolic enzymes. For example, TGF-β, a major driver of EMT, activates fatty acid synthase (FASN) and forms a FASN-TGFβ1-FASN positive loop in cisplatin-resistant cells, resulting in EMT induction(Hua et al., 2020; Jiang et al., 2015; Yang et al., 2016). However, the direct regulation of lipid enzymes by EMT factors remains to be elucidated. Herein, we demonstrated that the lipid rating-enzyme ACSL4 is a direct downstream target of the EMT transcription factor ZEB2 in controlling lipid metabolism. Mechanistically, ZEB2 activates ACSL4 mRNA expression by directly binding to its promoter, which contains four ZEB2 consensus sequences. Importantly, we observed a strong correlation between ZEB2 and ACSL4 expression levels in clinical breast cancer samples. ACSL4 re-expression rescues the migration ability of ZEB2-depleted cells. These observations indicated that ACSL4 is crucial for ZEB2-mediated metastasis.

We also demonstrated that ACSL4 directly binds to and stabilizes ZEB2 by reducing its ubiquitination. Our results are consistent with a recent report that ACSL4 stabilizes the oncoprotein c-Myc via the ubiquitin-proteasome system(Chen et al., 2020). We propose that as an LD enzyme, ACSL4 may participate in the protein degradation system of LD. This is likely to be a novel function of ACSL4. Interestingly, a recent study reported that lipid droplets recruit Numb through the AP2A/ACSL3 complex to promote Numb degradation(Liu et al., 2022). Thus, it is likely that lipid droplets act as a platform for protein degradation. Additionally, ACSL4 promoted ZEB2 expression as the mRNA level of ZEB2 was significantly reduced after ACSL4 knockdown. Therefore, ACSL4 regulates ZEB2 not only via a post-transcriptional mechanism but also via a transcriptional mechanism. Notably, the relationship between ZEB2 and ACSL4 could form a positive feedback loop: ZEB2 transcriptionally activates ACSL4, and conversely, ACSL4 stabilizes the ZEB2 protein by reducing its ubiquitination.

585 Amplification of either gene might therefore lock this loop in an active state, resulting
586 in the enhanced invasive and metastatic capabilities of breast cancer cells (Fig. 8G).
587
588 Previous studies have reported that ACSL4 could act as a tumor suppressor or
589 oncogene, depending on the specific cancer type and tissue environment(Cheng et
590 al., 2020; Grube et al., 2022; Lei et al., 2020; Ma et al., 2021; Zhang et al., 2021).
591 Indeed, ACSL4 could either be located at the cytomembrane or at the lipid droplets
592 and endoplasmic reticulum membrane, indicating the different functions of
593 ACSL4(Quan et al., 2021). The cytomembrane ACSL4 is likely responsible for
594 dictating ferroptosis sensitivity by shaping the plasma membrane lipidome, whereas
595 ACSL4 localized to lipid droplets has other functions. We provide evidence that
596 ACSL4, which is located in lipid droplets, is a pro-metastatic factor that promotes
597 invasion and migration. Notably, we demonstrated that ACSL4 depletion significantly
598 suppressed the invasion and migration of breast cancer cells in vitro and in vivo.
599 Furthermore, ACSL4 and ZEB2 were found to be preferentially expressed in
600 basal-like breast cancer cells and clinical samples that lacked ERα expression,
601 indicating that they are promising targets for highly invasive breast cancer. Survival
602 analysis revealed that high expression of ACSL4 or ZEB2 is associated with worse
603 post-progression survival than low expression in patients with breast cancer. It is
604 worth noting that there was no difference in the overall survival between ACSL4 or
605 ZEB2 high- and low-expression breast cancer patients (Supplementary Fig. S2),
606 suggesting that ACSL4 and ZEB2 could specifically be used as prognostic markers
607 for advanced breast cancer, and these axes hold promise as new metabolic
608 therapeutic targets for advanced breast cancer.
609
610 Although ACSL4 has been shown to play an essential role in metastasis in many
611 types of cancer (Maloberti et al., 2010; Sanchez-Martinez et al., 2017; Wu et al.,
612 2015), its mechanism of ACSL4-mediated metastasis is not fully understood. ACSL4
613 is a member of the long-chain fatty acetyl-CoA synthetase enzyme family that
614 catalyzes fatty acids to their active form, acyl-CoA, which can be directed to
615 anabolism or catabolism, depending on the cellular background. We observed that
616 the knockdown of ACSL4 significantly reduced the number and size of LD, indicating
617 that fatty acids were directed to anabolism to form LD by ACSL4. Indeed, it has been
618 shown that fatty acids are stored in LD before entering fatty acid oxidation, and the
619 formation of LD is required for fatty acids oxidation (Li et al., 2020; Petan, 2020; Welte
620 and Gould, 2017). This is in line with our observation that exogenous fatty acids (oleic
621 acid) significantly enhance lipid droplet accumulation and migration. Importantly,
622 lipidomic analysis revealed that the knockdown of ACSL4 significantly decreased the
623 incorporation of both saturated and unsaturated fatty acids into different species of
624 lipids, including triacylglycerols (TAG), phospholipids (PE, PC), and cholesteryl esters
625 (CE). Consistently, Frozen tissue sections from a metastatic animal model confirmed
626 that high ACSL4 expression was accompanied by apparent LD accumulation. These
627 results suggest that ACSL4 is a crucial regulator that promotes lipid storage during
628 breast cancer metastasis. Interestingly, knockdown of ACSL4 restored the expression

629 of E-cadherin, an essential adhesion molecule, indicating that ACSL4 promotes tumor
630 invasion through multiple mechanisms.
631
632 Reprogramming of lipid metabolism is an essential step in metastasis. Lipid droplets
633 are highly dynamic monolayer membrane-bound organelles involved in energy
634 utilization, signal transduction, and cancer invasion. The number and size of LD are
635 associated with cancer aggressiveness(Cruz et al., 2020). We observed that highly
636 invasive breast cancer cells were enriched with LD. Using fluorescence microscopy,
637 we noticed that the number of LD was significantly reduced after cell migration. Our
638 findings are in line with a recent study showing that LD undergo lipolysis during the
639 process of migration in pancreatic cancer(Rozeveld et al., 2020). It is likely that fatty
640 acids are released from lipid droplets and form acyl-CoA, which enters OXPHOS to
641 support the energy needed for metastasis. Therefore, these data support the notion
642 that increased LD accumulation is a priming state prior to metastasis, and that LD are
643 crucial resources to fuel the process of metastasis.
644
645 In addition, we observed that ACSL4 also participates in FA catabolism, as the
646 long-chain fatty acid-derived OCR rate and ATP production were significantly reduced
647 in ACSL4-depleted cells, indicating that ACSL4 is essential for FAO stimulation. Our
648 results are in line with a recent study that reported that hexokinase 2 enhances
649 tumorigenicity by activating the ACSL4-mediated fatty acid β-oxidation pathway (Li et
650 al., 2022). Notably, the expression of CPT1, a rate-limiting enzyme of FAO, was
651 significantly reduced in the ACSL4-depleted cells. Among the three isoforms of CPT1,
652 CPT1A is the only isoform regulated by ACSL4. We proposed that ACSL4 promotes
653 FAO and ATP production by upregulating CPT1A, thereby providing energy support
654 for breast cancer metastasis. Our results reveal the mechanism of previous findings
655 that FAO is a critical energy pathway in triple-negative breast cancer
656 (TNBC)(Camarda et al., 2016). In addition to the finding that ACSL4 promotes FAO to
657 fuel metastasis, we observed that lactate levels did not change after ACSL4
658 knockdown, suggesting that glycolysis is not involved in ACSL4-mediated energy
659 metabolism. Therefore, we propose a model in which cell migration is a multistep
660 process accompanied by dynamic cellular lipid metabolic changes. At the
661 pre-metastatic stage, ACSL4 enhances LD accumulation by promoting lipogenesis.
662 During metastasis, ACSL4 stimulates fatty acid oxidation to generate adenosine
663 triphosphate (ATP).
664
665 In conclusion, we provide insights into the mechanistic links between EMT and lipid
666 metabolism and identify the ZEB2/ACSL4 axis as a novel metastatic metabolic
667 pathway that stimulates both lipogenesis and fatty acid oxidation, resulting in
668 enhanced breast cancer invasion and metastasis. Importantly, our results
669 demonstrate that ACSL4 is a direct downstream target of ZEB2 in controlling lipid
670 storage and LD accumulation, which are important steps and energy pools for
671 metastasis. Clinically, our findings identified ZEB2-ACSL4 signalling as an attractive
672 therapeutic target for overcoming breast cancer metastasis. Elevated ACSL4 levels

can be used as an effective marker for predicting cancer progression in patients with advanced breast cancer.

Additional information

Funding

Funder	Grant reference number	Author
Guangzhou Science and Technology Project	202201020240	Na Yang
Medical Research Foundation of Guangdong Province	A2021112	Na Yang
National Natural Science Foundation of China	81602434	Na Yang
Research Agreement between South China University of Technology and Guangzhou First People's Hospital	D9194290	Yuyou Duan
National Natural Science Foundation of China	81972594	Min Yan

The funders had no role in study design, data collection and interpretation, or the decision to submit the work for publication.

Acknowledgements:

We acknowledge Professors Quentin Liu for the paclitaxel-resistant and epirubicin-resistant MCF-7 cell lines and Dr. Jue Wang and Dr. Peilin Liao for their technical support. We thank all members of Professor YY. Duan's lab for helpful insights and valuable advice.

Authors' Contributions:

N. Yang and J. Lin designed the study. J. Lin, P. Zhang, J. Zhang, and W. Liu performed experiments. W. Liu and G. Liu provided the clinical samples. N. Yang, J. Lin, and P. Zhang analyzed the data. N. Yang, J. Lin, M. Yan, and Y. Duan wrote and revised the manuscript. N. Yang, M. Yan and Y. Duan provided financial support.

Disclosure of Potential Conflicts of Interest

The authors declare no potential conflicts of interest.

Reference

Antunes, P., Cruz, A., Barbosa, J., Bonifacio, V.D.B., and Pinto, S.N. 2022. Lipid Droplets in Cancer: From Composition and Role to Imaging and Therapeutics. Molecules *27*. DOI: 10.3390/molecules27030991, PMID:35164256

Barzaman, K., Karami, J., Zarei, Z., Hosseinzadeh, A., Kazemi, M.H., Moradi-Kalbolandi, S., Safari, E., and Farahmand, L. 2020. Breast cancer: Biology, biomarkers, and treatments. Int Immunopharmacol *84*, 106535. DOI: 10.1016/j.intimp.2020.106535, PMID:32361569

Bian, X., Liu, R., Meng, Y., Xing, D., Xu, D., and Lu, Z. 2021. Lipid metabolism and cancer. J Exp Med *218*. DOI: 10.1084/jem.20201606, PMID:33601415

Camarda, R., Zhou, A.Y., Kohnz, R.A., Balakrishnan, S., Mahieu, C., Anderton, B., Eyob, H., Kajimura, S., Tward, A., Krings, G.*, et al.* 2016. Inhibition of fatty acid oxidation as a therapy for MYC-overexpressing triple-negative breast cancer. Nat Med *22*, 427-432. DOI: 10.1038/nm.4055, PMID:26950360

Chen, J., Ding, C., Chen, Y., Hu, W., Lu, Y., Wu, W., Zhang, Y., Yang, B., Wu, H., Peng, C.*, et al.* 2020. ACSL4 promotes hepatocellular carcinoma progression via c-Myc stability mediated by ERK/FBW7/c-Myc axis. Oncogenesis *9*, 42. DOI: 10.1038/s41389-020-0226-z, PMID:32350243

Cheng, C., Geng, F., Cheng, X., and Guo, D. 2018. Lipid metabolism reprogramming and its potential targets in cancer. Cancer Commun (Lond) *38*, 27. DOI: 10.1186/s40880-018-0301-4, PMID:29784041

Cheng, J., Fan, Y.Q., Liu, B.H., Zhou, H., Wang, J.M., and Chen, Q.X. 2020. ACSL4 suppresses glioma cells proliferation via activating ferroptosis. Oncol Rep *43*, 147-158. DOI: 10.3892/or.2019.7419, PMID:31789401

Corbet, C., Bastien, E., Santiago de Jesus, J.P., Dierge, E., Martherus, R., Vander Linden, C., Doix, B., Degavre, C., Guilbaud, C., Petit, L.*, et al.* 2020. TGFbeta2-induced formation of lipid droplets supports acidosis-driven EMT and the metastatic spreading of cancer cells. Nat Commun *11*, 454. DOI: 10.1038/s41467-019-14262-3, PMID:31974393

Cruz, A.L.S., Barreto, E.A., Fazolini, N.P.B., Viola, J.P.B., and Bozza, P.T. 2020. Lipid droplets: platforms with multiple functions in cancer hallmarks. Cell Death Dis *11*, 105. DOI: 10.1038/s41419-020-2297-3, PMID:32029741

Doll, S., Proneth, B., Tyurina, Y.Y., Panzilius, E., Kobayashi, S., Ingold, I., Irmler, M., Beckers, J., Aichler, M., Walch, A.*, et al.* 2017. ACSL4 dictates ferroptosis sensitivity by shaping cellular lipid composition. Nat Chem Biol *13*, 91-98. DOI: 10.1038/nchembio.2239, PMID:27842070

Dongre, A., and Weinberg, R.A. 2019. New insights into the mechanisms of epithelial-mesenchymal transition and implications for cancer. Nat Rev Mol Cell Biol *20*, 69-84. DOI: 10.1038/s41580-018-0080-4, PMID:30459476

Fahad Ullah, M. 2019. Breast Cancer: Current Perspectives on the Disease Status. Adv Exp Med Biol *1152*, 51-64. DOI: 10.1007/978-3-030-20301-6_4, PMID:31456179

Grube, J., Woitok, M.M., Mohs, A., Erschfeld, S., Lynen, C., Trautwein, C., and Otto, T. 2022. ACSL4-dependent ferroptosis does not represent a tumor-suppressive mechanism but ACSL4 rather promotes liver cancer progression. Cell Death Dis *13*, 704. DOI: 10.1038/s41419-022-05137-5, PMID:35963845

Hua, W., Ten Dijke, P., Kostidis, S., Giera, M., and Hornsveld, M. 2020. TGFbeta-induced metabolic reprogramming during epithelial-to-mesenchymal transition in cancer. Cell Mol Life Sci *77*, 2103-2123. DOI: 10.1007/s00018-019-03398-6, PMID:31822964

Huang, W.C., Li, X., Liu, J., Lin, J., and Chung, L.W. 2012. Activation of androgen receptor, lipogenesis, and oxidative stress converged by SREBP-1 is responsible for regulating growth and progression of prostate cancer cells. Mol Cancer Res *10*, 133-142. DOI: 10.1158/1541-7786.MCR-11-0206, PMID:22064655

Jiang, L., Xiao, L., Sugiura, H., Huang, X., Ali, A., Kuro-o, M., Deberardinis, R.J., and Boothman, D.A. 2015. Metabolic reprogramming during TGFbeta1-induced

epithelial-to-mesenchymal transition. Oncogene *34*, 3908-3916. DOI: 10.1038/onc.2014.321, PMID:25284588

Jin, C., and Yuan, P. 2020. Implications of lipid droplets in lung cancer: Associations with drug resistance. Oncol Lett *20*, 2091-2104. DOI: 10.3892/ol.2020.11769, PMID:32782526

Kang, H., Kim, H., Lee, S., Youn, H., and Youn, B. 2019. Role of Metabolic Reprogramming in Epithelial(-)Mesenchymal Transition (EMT). Int J Mol Sci *20*. DOI: 10.3390/ijms20082042, PMID:31027222

Kuwata, H., and Hara, S. 2019. Role of acyl-CoA synthetase ACSL4 in arachidonic acid metabolism. Prostaglandins Other Lipid Mediat *144*, 106363. DOI: 10.1016/j.prostaglandins.2019.106363, PMID:31306767

Lei, G., Zhang, Y., Koppula, P., Liu, X., Zhang, J., Lin, S.H., Ajani, J.A., Xiao, Q., Liao, Z., Wang, H.*, et al.* 2020. The role of ferroptosis in ionizing radiation-induced cell death and tumor suppression. Cell Res *30*, 146-162. DOI: 10.1038/s41422-019-0263-3, PMID:31949285

Li, H., Song, J., He, Y., Liu, Y., Liu, Z., Sun, W., Hu, W., Lei, Q.Y., Hu, X., Chen, Z.*, et al.* 2022. CRISPR/Cas9 Screens Reveal that Hexokinase 2 Enhances Cancer Stemness and Tumorigenicity by Activating the ACSL4-Fatty Acid beta-Oxidation Pathway. Adv Sci (Weinh) *9*, e2105126. DOI: 10.1002/advs.202105126, PMID:35603967

Li, Z., Liu, H., and Luo, X. 2020. Lipid droplet and its implication in cancer progression. Am J Cancer Res *10*, 4112-4122. DOI: PMID:33414989

Liu, H., Du, J., Chao, S., Li, S., Cai, H., Zhang, H., Chen, G., Liu, P., and Bu, P. 2022. Fusobacterium nucleatum Promotes Colorectal Cancer Cell to Acquire Stem Cell-Like Features by Manipulating Lipid Droplet-Mediated Numb Degradation. Adv Sci (Weinh) *9*, e2105222. DOI: 10.1002/advs.202105222, PMID:35170250

Luo, X., Cheng, C., Tan, Z., Li, N., Tang, M., Yang, L., and Cao, Y. 2017. Emerging roles of lipid metabolism in cancer metastasis. Mol Cancer *16*, 76. DOI: 10.1186/s12943-017-0646-3, PMID:28399876

Luond, F., Sugiyama, N., Bill, R., Bornes, L., Hager, C., Tang, F., Santacroce, N., Beisel, C., Ivanek, R., Burglin, T.*, et al.* 2021. Distinct contributions of partial and full EMT to breast cancer malignancy. Dev Cell *56*, 3203-3221 e3211. DOI: 10.1016/j.devcel.2021.11.006, PMID:34847378

Ma, L.L., Liang, L., Zhou, D., and Wang, S.W. 2021. Tumor suppressor miR-424-5p abrogates ferroptosis in ovarian cancer through targeting ACSL4. Neoplasma *68*, 165-173. DOI: 10.4149/neo_2020_200707N705, PMID:33038905

Maan, M., Peters, J.M., Dutta, M., and Patterson, A.D. 2018. Lipid metabolism and lipophagy in cancer. Biochem Biophys Res Commun *504*, 582-589. DOI: 10.1016/j.bbrc.2018.02.097, PMID:29438712

Maloberti, P.M., Duarte, A.B., Orlando, U.D., Pasqualini, M.E., Solano, A.R., Lopez-Otin, C., and Podesta, E.J. 2010. Functional interaction between acyl-CoA synthetase 4, lipooxygenases and cyclooxygenase-2 in the aggressive phenotype of breast cancer cells. PLoS One *5*, e15540. DOI: 10.1371/journal.pone.0015540, PMID:21085606

Mittal, V. 2018. Epithelial Mesenchymal Transition in Tumor Metastasis. Annu Rev Pathol *13*, 395-412. DOI: 10.1146/annurev-pathol-020117-043854, PMID:29414248

Mosier, J.A., Schwager, S.C., Boyajian, D.A., and Reinhart-King, C.A. 2021. Cancer cell metabolic plasticity in migration and metastasis. Clin Exp Metastasis *38*, 343-359. DOI:

10.1007/s10585-021-10102-1, PMID:34076787

Niu, Z., Chen, G., Chang, W., Sun, P., Luo, Z., Zhang, H., Zhi, L., Guo, C., Chen, H., Yin, M.*, et al.* 2021. Chimeric antigen receptor-modified macrophages trigger systemic anti-tumour immunity. J Pathol *253*, 247-257. DOI: 10.1002/path.5585, PMID:33140856

Orlando, U.D., Castillo, A.F., Medrano, M.A.R., Solano, A.R., Maloberti, P.M., and Podesta, E.J. 2019. Acyl-CoA synthetase-4 is implicated in drug resistance in breast cancer cell lines involving the regulation of energy-dependent transporter expression. Biochem Pharmacol *159*, 52-63. DOI: 10.1016/j.bcp.2018.11.005, PMID:30414939

Park, M., Kim, D., Ko, S., Kim, A., Mo, K., and Yoon, H. 2022. Breast Cancer Metastasis: Mechanisms and Therapeutic Implications. Int J Mol Sci *23*. DOI: 10.3390/ijms23126806, PMID:35743249

Petan, T. 2020. Lipid Droplets in Cancer. Rev Physiol Biochem Pharmacol. DOI: 10.1007/112_2020_51, PMID:33074407

Quan, J., Bode, A.M., and Luo, X. 2021. ACSL family: The regulatory mechanisms and therapeutic implications in cancer. Eur J Pharmacol *909*, 174397. DOI: 10.1016/j.ejphar.2021.174397, PMID:34332918

Roman, M., Wrobel, T.P., Panek, A., Paluszkiewicz, C., and Kwiatek, W.M. 2020. Lipid droplets in prostate cancer cells and effect of irradiation studied by Raman microspectroscopy. Biochim Biophys Acta Mol Cell Biol Lipids *1865*, 158753. DOI: 10.1016/j.bbalip.2020.158753, PMID:32504818

Rossi Sebastiano, M., and Konstantinidou, G. 2019. Targeting Long Chain Acyl-CoA Synthetases for Cancer Therapy. Int J Mol Sci *20*. DOI: 10.3390/ijms20153624, PMID:31344914

Rozeveld, C.N., Johnson, K.M., Zhang, L., and Razidlo, G.L. 2020. KRAS Controls Pancreatic Cancer Cell Lipid Metabolism and Invasive Potential through the Lipase HSL. Cancer Res *80*, 4932-4945. DOI: 10.1158/0008-5472.CAN-20-1255, PMID:32816911

Sanchez-Martinez, R., Cruz-Gil, S., Garcia-Alvarez, M.S., Reglero, G., and Ramirez de Molina, A. 2017. Complementary ACSL isoforms contribute to a non-Warburg advantageous energetic status characterizing invasive colon cancer cells. Sci Rep *7*, 11143. DOI: 10.1038/s41598-017-11612-3, PMID:28894242

Sciacovelli, M., and Frezza, C. 2017. Metabolic reprogramming and epithelial-to-mesenchymal transition in cancer. FEBS J *284*, 3132-3144. DOI: 10.1111/febs.14090, PMID:28444969

Senga, S., Kobayashi, N., Kawaguchi, K., Ando, A., and Fujii, H. 2018. Fatty acid-binding protein 5 (FABP5) promotes lipolysis of lipid droplets, de novo fatty acid (FA) synthesis and activation of nuclear factor-kappa B (NF-kappaB) signaling in cancer cells. Biochim Biophys Acta Mol Cell Biol Lipids *1863*, 1057-1067. DOI: 10.1016/j.bbalip.2018.06.010, PMID:29906613

Snaebjornsson, M.T., Janaki-Raman, S., and Schulze, A. 2020. Greasing the Wheels of the Cancer Machine: The Role of Lipid Metabolism in Cancer. Cell Metab *31*, 62-76. DOI: 10.1016/j.cmet.2019.11.010, PMID:31813823

Soukupova, J., Malfettone, A., Bertran, E., Hernandez-Alvarez, M.I., Penuelas-Haro, I., Dituri, F., Giannelli, G., Zorzano, A., and Fabregat, I. 2021. Epithelial-Mesenchymal Transition (EMT) Induced by TGF-beta in Hepatocellular Carcinoma Cells Reprograms Lipid Metabolism. Int J Mol Sci *22*. DOI: 10.3390/ijms22115543, PMID:34073989

832 Taib, B., Aboussalah, A.M., Moniruzzaman, M., Chen, S., Haughey, N.J., Kim, S.F., and Ahima,
833 R.S. 2019. Lipid accumulation and oxidation in glioblastoma multiforme. Sci Rep *9*, 19593.
834 DOI: 10.1038/s41598-019-55985-z, PMID:31863022
835 Welte, M.A., and Gould, A.P. 2017. Lipid droplet functions beyond energy storage. Biochim
836 Biophys Acta Mol Cell Biol Lipids *1862*, 1260-1272. DOI: 10.1016/j.bbalip.2017.07.006,
837 PMID:28735096
838 Wright, H.J., Hou, J., Xu, B., Cortez, M., Potma, E.O., Tromberg, B.J., and Razorenova, O.V.
839 2017. CDCP1 drives triple-negative breast cancer metastasis through reduction of lipid-droplet
840 abundance and stimulation of fatty acid oxidation. Proc Natl Acad Sci U S A *114*, E6556-E6565.
841 DOI: 10.1073/pnas.1703791114, PMID:28739932
842 Wu, X., Deng, F., Li, Y., Daniels, G., Du, X., Ren, Q., Wang, J., Wang, L.H., Yang, Y., Zhang, V.*,*
843 *et al.* 2015. ACSL4 promotes prostate cancer growth, invasion and hormonal resistance.
844 Oncotarget *6*, 44849-44863. DOI: 10.18632/oncotarget.6438, PMID:26636648
845 Yang, L., Zhang, F., Wang, X., Tsai, Y., Chuang, K.H., Keng, P.C., Lee, S.O., and Chen, Y.
846 2016. A FASN-TGF-beta1-FASN regulatory loop contributes to high EMT/metastatic potential
847 of cisplatin-resistant non-small cell lung cancer. Oncotarget *7*, 55543-55554. DOI:
848 10.18632/oncotarget.10837, PMID:27765901
849 Yang, N., Wang, C., Wang, Z., Zona, S., Lin, S.X., Wang, X., Yan, M., Zheng, F.M., Li, S.S., Xu,
850 B.*, et al.* 2017. FOXM1 recruits nuclear Aurora kinase A to participate in a positive feedback
851 loop essential for the self-renewal of breast cancer stem cells. Oncogene *36*, 3428-3440.
852 DOI: 10.1038/onc.2016.490, PMID:28114286
853 Zembroski, A.S., Andolino, C., Buhman, K.K., and Teegarden, D. 2021. Proteomic
854 Characterization of Cytoplasmic Lipid Droplets in Human Metastatic Breast Cancer Cells.
855 Front Oncol *11*, 576326. DOI: 10.3389/fonc.2021.576326, PMID:34141606
856 Zhang, Y., Li, S., Li, F., Lv, C., and Yang, Q.K. 2021. High-fat diet impairs ferroptosis and
857 promotes cancer invasiveness via downregulating tumor suppressor ACSL4 in lung
858 adenocarcinoma. Biol Direct *16*, 10. DOI: 10.1186/s13062-021-00294-7, PMID:34053456
859 Zheng, F.M., Long, Z.J., Hou, Z.J., Luo, Y., Xu, L.Z., Xia, J.L., Lai, X.J., Liu, J.W., Wang, X.,
860 Kamran, M.*, et al.* 2014. A novel small molecule aurora kinase inhibitor attenuates breast
861 tumor-initiating cells and overcomes drug resistance. Mol Cancer Ther *13*, 1991-2003. DOI:
862 10.1158/1535-7163.MCT-13-1029, PMID:24899685
863

864 **Figure Legends**

865 **Figure 1,** The expression and relationship of ZEB2 and ACSL4 in breast cancer. **A,** Heat
866 maps of the 38 up-regulated EMT-related genes detected by RNA-seq analysis in the
867 paclitaxel-resistant MCF-7 cell line (TAXOL) and Epirubicin-resistant MCF-7 cell line (EPI)
868 compared to wild-type MCF-7 cell line. **B,** The correlation between ACSL4 and ZEB2
869 mRNA expression in the TCGA cohort consisting of 1222 breast cancer patient samples.
870 Spearman correlation and linear regression analysis were employed. **C,** The correlation
871 between ACSL4 and ERα mRNA expression in the TCGA cohort consisting of 666 breast
872 cancer patient samples. Spearman correlation and linear regression analysis were
873 employed. **D,** PPS (post-progression survival) was examined by Kaplan–Meier analysis to
874 compare the survival rates in ACSL high and low expression of breast cancer patients. **E,**

875 PPS (post-progression survival) was examined by Kaplan–Meier analysis to compare the
876 survival rates in ZEB2 high and low expression of breast cancer patients. **F,** Expression of
877 ACSL4 and ZEB2 were analyzed by western blot in a panel of 5 breast cancer cell lines,
878 including two basal-like, two luminal and one taxol-resistant cell. **G,** Expression of ACSL4
879 and ZEB2 were analyzed by western blot in a panel of nine cases of tumour samples,
880 including 5 cases of luminal (Patient 1, 2, 3, 4, 5) and 4 cases of triple-negative breast
881 cancer (Patient 6, 7, 8, 9). **H,** Scatter plot with linear regression analysis from expression
882 level of G. **I,** HE staining and IHC analysis of ACSL4, ZEB2, ERα expression in
883 representative basal-like and luminal subtype breast cancer tissues. Representative
884 pictures were shown. Scale bar, 50 μm.
885
886 **Figure 2,** Over-expression of ACSL4 contributes to ZEB2-mediated breast cancer
887 invasion. **A,** Cell metastatic capacity was analyzed by wound healing assay in control or
888 ACSL4 over-expression MCF-7 cells (Left panel). Quantification of relative migration
889 distance (Right panel). Scale bar, 5mm. **B,** Cell invasive capacity was analyzed by
890 transwell invasion assay in control or ACSL4 over-expression MCF-7 cells (Left panel).
891 Quantification of relative migration distance (Right panel). Scale bar, 1mm. **C,** Cell
892 metastatic capacity was analyzed by wound healing assays in control or ACSL4 silencing
893 MDA-MD-231 cells (shACSL4) (Left panel). Quantification of relative migration distance
894 (Right panel). Scale bar, 5mm. **D,** Cell invasive capacity was analyzed by transwell
895 invasion assay in control or ACSL4 silencing MDA-MD-231 cells (shACSL4) (Left panel).
896 Quantification of relative migration distance (Right panel). Scale bar, 1mm. **E,** KEGG
897 pathway enrichment analysis of differentially expressed genes by RNA-sequencing
898 between control and ACSL4 knockdown MDA-MB-231 cells. The top 10 deferential
899 pathways were listed. **F,** Expression of three EMT-related genes, E-cadherin, N-cadherin,
900 and vimentin, was analyzed by western blotting in control, ACSL4, or ZEB2 silencing
901 MDA-MB-231 cells. **G,** Cell invasive and metastatic capacity were analyzed by transwell
902 invasion assay and wound healing assays (Scale bar, 5mm) in control and ZEB2
903 knockdown, or ZEB2 knockdown cells that over-express ACSL4. **H,** Graphs indicated the
904 Statistical analysis in G analyzed by Student's t-test (mean ± SEM). ** $P<0.01$, ***
905 $P<0.001$, **** $P<0.0001$. All results are from three or four independent experiments.
906
907 **Figure 3,** ACSL4 promotes lipid droplets accumulation and lipogenesis. **A,** BODIPY
908 493/503 staining of lipid droplets in MCF-7, Taxol-resistant MCF-7 cells (TAXOL-7), or
909 MDA-MB-231 cells (Left panel). Quantification of normalized lipid contents (Right panel).
910 Scale bar, 5μm. **B,** BODIPY 493/503 staining of lipid droplets in control or ACSL4
911 knockout MDA-MB-231 cells (Upper panel). Quantification of normalized fluorescence
912 intensity and percentage of LD-containing cell number (Lower panel). Scale bar, 50μm. **C,**
913 BODIPY 493/503 staining of lipid droplets in control or ZEB2 knockout MDA-MB-231 cells
914 (Upper panel). Quantification of normalized fluorescence intensity and percentage of
915 LD-containing cell number (Lower panel). Scale bar, 50μm. **D,** The heatmap of
916 representative down-regulated lipid species (TG, PE, PC) with hierarchical clustering in
917 the control cells and ACSL4 Knockdown cells. Each species was normalized to the

corresponding mean value, as determined by two-way ANOVA. **E,** Quantification of different FA containing TG, PC, and PE species in control or ACSL4 Knockdown MDA-MD-231 cells. * P<0.05, ** P<0.01, *** P<0.001, **** P<0.0001. Error bars, SD.

Figure 4, Exogenous lipids promote LD accumulation and fuel cell migration. **A,** BODIPY 493/503 staining of lipid droplets in control cells or oleic acid (OA) loaded (200 μM) MDA-MB-231 cells. Scale bar, 10 μm. **B,** Quantification of normalized lipid contents from the conditions in (A). **C,** Cell invasive capacity was analyzed by transwell invasion assay in control or oleic acid (OA) loaded (200 μM) MDA-MB-231 cells. Cells invaded for 16 hours through a Matrigel-coated filter toward high-serum media (Left panel). Quantification of relative invasive cells (Right panel). Scale bar, 1 mm. **D,** Cell metastatic capacity was analyzed by wound healing assays in control or oleic acid (OA) loaded (200 μM) MDA-MB-231 cells. Scale bar, 5 mm. **E,** Cells were seeded in a transwell chamber. After 24 hours, cells migrated to the lower side of the chamber, and the fluorescence intensity per cell was calculated (Left panel). Quantitation of total LD area per cell before and after cell migration (Right panel). Scale bar, 10 μm (small) and 50 μm (big). *** P<0.001, **** P<0.0001.

Figure 5, ACSL4 and ZEB2 increase fatty acid oxygen consumption and promote ATP generation in BLBC Cells. **A,** Reactome pathway analysis of differentially expressed genes by RNA-sequencing between control and ACSL4 knockdown MDA-MB-231 cells. The representative pathways were shown. **B,** Heatmap showing the differentially expressed genes between control cells and ACSL4 knockdown cells. The representative FAO-related genes were shown. **C,** The mRNA levels of CPT1A, CPT1B, and CPT1C were analyzed by quantitative PCR in control and ACSL4 knockdown cells. **D,** Quantitation of the normalized oxygen consumption rate (OCR) for long-chain fatty acids was monitored by Agilent XF Substrate Oxidation Stress Test in control or ACSL4 knockdown cells. Specific inhibitors were added as indicated. **E,** Quantitation of the normalized oxygen consumption rate (OCR) for long-chain fatty acids was monitored by Agilent XF Substrate Oxidation Stress Test in control or ZEB2 knockdown cells. Specific inhibitors were added as indicated. **F and G,** ATP production was quantified in control or ACSL4 knockdown cells (Left) or ZEB2 knockdown cells (Right). **H and I,** Lactate production was examined in control and ACSL4 knockdown (shACSL4) or ZEB2 knockdown (shZEB2) cells. Data are represented as mean SEM of three independent experiments, analyzed by Student's t-test, * P<0.05, **** P<0.0001.

Figure 6, ZEB2 activates ACSL4 expression by directly binding to its promoter. **A,** Relative mRNA levels of ZEB2 and ACSL4 in control or ZEB2 knockdown MDA-MB-231 cells. **B,** Protein levels of ZEB2 and ACSL4 in control or ZEB2 knockdown MDA-MB-231 cells. **C and D,** Truncated ACSL4 promoter segment activity analyzed by Luciferase reporter assay in control or ZEB2 over-expressed 293T cells. **E,** The specific primers designed for ACSL4 promoter according to the E-box position shown in C (set1 to -287bp, set2 to -995, set3 to -1038, set4 to -1116). **F,** ChIP assay analysis of the occupation of ZEB2 on ACSL4 promoter by using four primers as indicated in E. **G,** Quantitative PCR

962 analysis of ZEB2-binding abundance of specific ACSL4 promoter region by using set1
963 primer indicated in F. Genomic DNA was purified after chromatin immunoprecipitation and
964 analyzed by Quantitative PCR. **H,** Luciferase reporter analysis of the activity of wild-type
965 ACSL4 promoter or its mutants in control or ZEB2 over-expression 293T cells. Data are
966 represented as mean SD of three independent experiments, analyzed by Student's t-test,
967 ** P<0.01, *** P<0.001, **** P<0.0001.
968
969 **Figure 7,** ACSL4 regulates ZEB2 mRNA expression and protein stability. **A,** Relative
970 mRNA levels of ZEB2 and ACSL4 in control or ACSL4 silencing MDA-MB-231 cells. **B,**
971 Protein levels of ZEB2 and ACSL4 in control or ACSL4 silencing MDA-MB-231 cells as
972 indicated. **C,** Ubiquitylation of ZEB2 was examined by in vitro ubiquitin assay. 293T cells
973 were co-transfected with indicated constructs. Cells were treated with MG132 for 6 hours
974 before IP. Anti-MYC was used to pull down the ZEB2 protein. The polyubiquitinated ZEB2
975 protein was detected by an anti-HA antibody. **D,** The interaction between ACSL4 and
976 ZEB2 was detected by Co-IP assay. 293T cells were co-transfected with ZEB2 and
977 ACSL4 expressing construct. Anti-HA antibody was used to pull down the protein. **E**, The
978 stability of ZEB2 protein was detected by CHX treatment assay in control or ACSL4
979 silencing MDA-MB-231 cells. Cells were treated with 100 μg/mL cycloheximide (CHX) and
980 were harvested at the indicated times after the addition of CHX. GAPDH was used as the
981 internal loading control. **F,** Quantification of stability assays shown in E. **G,** The stability of
982 ZEB2 protein was detected by CHX treatment assay in control or ACSL4 over-expressed
983 MDA-MB-231 cells. GAPDH was used as the internal loading control. **H,** Quantification of
984 stability assays shown in G. *** P<0.001.
985
986 **Figure 8,** ACSL4 knockdown attenuates lung metastasis of breast cancer. **A,** Cell
987 metastatic capacity was determined by xenograft experiment in vivo. Control cells and
988 ACSL4 knockdown MDA-MB-231 cells were mixed with Matrigel in a 1:1 ratio and injected
989 into NSG mice. Lung metastatic burden in mice was quantified by bioluminescence
990 imaging at the experimental endpoint (Left panel). Quantification of normalized gray area
991 (Right panel). **B,** Representative xenograft tumor images and HE staining pictures of
992 metastatic nodules in lungs (pointed by black arrows) were shown. The right panel shows
993 the quantification of metastatic lung nodules in two groups, as indicated. **C,** The image of
994 xenograft tumors developed from the control and ACSL4 knockdown cells. **D,** The tumor
995 volumes were measured and calculated at the indicated time. **E,** Representative IHC
996 images of lung metastatic lesions (Left panel) and quantification is shown (Right panel).
997 Scale. Bar, 50μm. **F,** The representative images of fluorescence assay for ACSL4 and lipid
998 droplets (Left panel). The fluorescence intensity of lipid droplets and ACSL4 were
999 calculated in the right panel. Scale. Bar, 100μm. **G,** A proposed mechanism to illustrate
1000 the positive feedback loop of ZEB2 and ACSL4 regulates lipid metabolism, which results
1001 in enhanced breast cancer metastasis. Data are represented as mean SEM of three
1002 independent experiments and analyzed by Student's t-test, * P<0.05, *** P<0.001, ****
1003 P<0.0001.
1004
1005 **Supplementary Figure Legends**

1006 **Supplementary Figure S1:** The representative differential genes between wild-type
1007 MCF-7 cells, paclitaxel-resistant MCF-7 cells (TAXOL), and Epirubicin-resistant MCF-7
1008 cells (EPI).
1009 **A,** The heat map of the up-regulated genes in drug-resistant cells was shown. **B,** The heat
1010 map of the down-regulated genes in the drug-resistant cell was shown.
1011
1012 **Supplementary Figure S2:** Overall survival of breast cancers was examined by Kaplan–
1013 Meier analysis to compare the survival rates between ACSL high- or ZEB2 high- and
1014 low-expression breast cancer patients.
1015
1016 **Supplementary Figure S3:** The metastatic and invasive capacities were reduced in
1017 ZEB2 knockdown MDA-MD-231 cells (shZEB2).
1018 **A,** Wound healing assays were performed in control cells or ZEB2 knockdown (shZEB2)
1019 MDA-MD-231 cells. Scale bar, 5 mm. **B,** Transwell invasive assay was performed in
1020 control cells or ZEB2 knockdown (shZEB2) MDA-MD-231 cells. Scale bar, 1 mm. ***
1021 P<0.001, **** P<0.0001.
1022
1023 **Supplementary Figure S4:** Fluorescence staining of lipid droplets and ACSL4 in
1024 MDA-MB-231 cells. Scale bar, 10 μm.
1025
1026 **Supplementary Figure S5:** ACSL4 regulates lipid composition in BLBC cells.
1027 **A,** The heat map of the down-regulated lipid species in ACSL4 knockdown cells
1028 (shACSL4) compared with those in control cells. **B,** Quantification of different species of
1029 lipids in two groups as indicated. * P<0.05, ** P<0.01.
1030
1031 **Supplementary Figure S6:** ACSL4 regulates the expression of lipid metabolic genes.
1032 **A.** Western blot analysis of CPT1A expression in control and ACSL4 knockdown, or ZEB2
1033 knockdown MDA-MD-231 cells. **B,** Relative mRNA levels of ATGL, FASN and SREBP2 in
1034 control or ACSL4 knockdown MDA-MB-231 cells (shACSL4). ** P<0.01, *** P<0.001.

Figure1

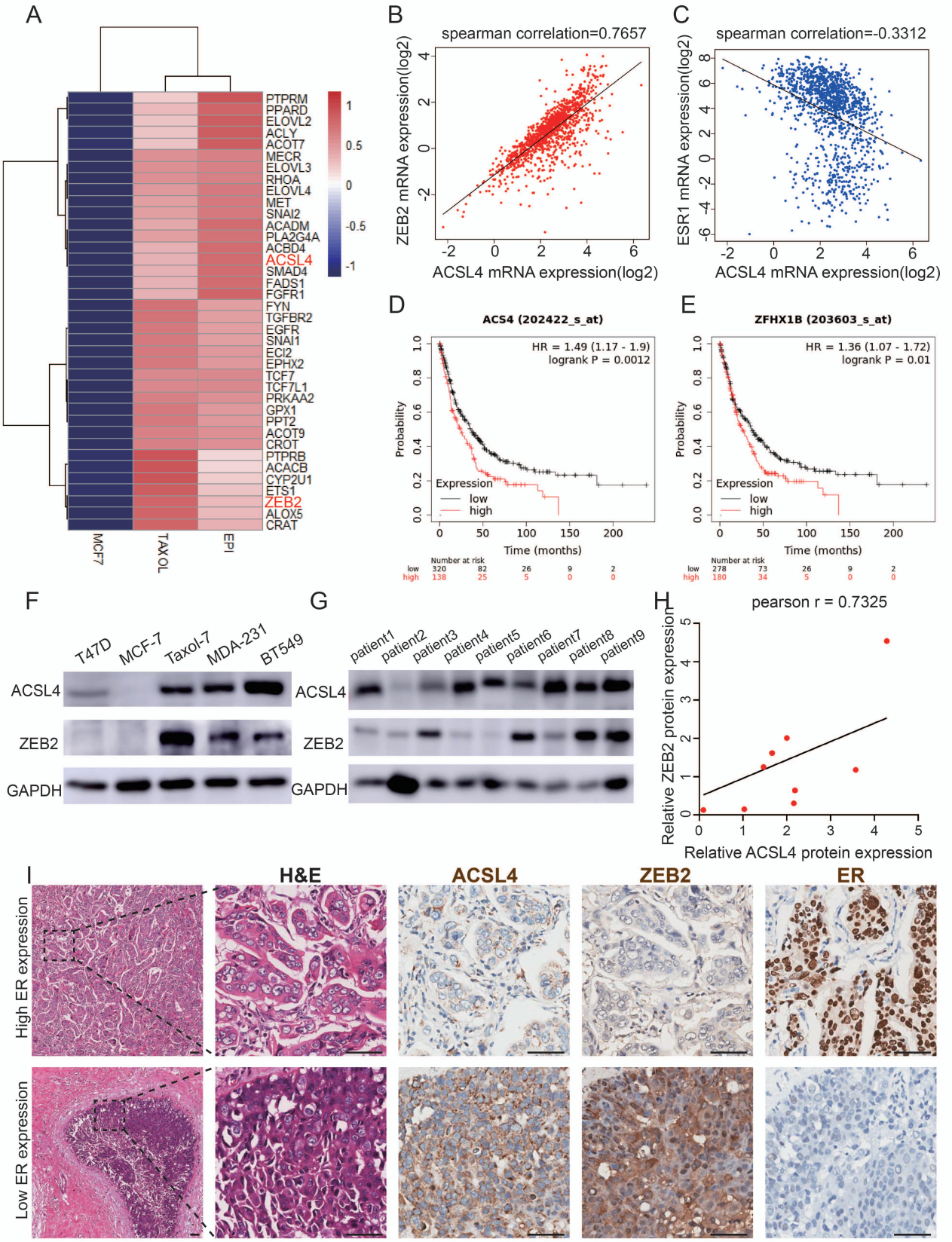
A
PTPRM
PPARD
ELOVL2
ACLY
ACOT7
MECR
ELOVL3
RHOA
ELOVL4
MET
SNAI2
ACADM
PLA2G4A
ACBD4
ACSL4
SMAD4
FADS1
FGFR1
FYN
TGFBR2
EGFR
SNAI1
ECI2
EPHX2
TCF7
TCF7L1
PRKAA2
GPX1
PPT2
ACOT9
CROT
PTPRB
ACACB
CYP2U1
ETS1
ZEB2
ALOX5
CRAT
MCF7
TAXOL
EPI
B
spearman correlation=0.7657
ZEB2 mRNA expression(log2)
ACSL4 mRNA expression(log2)
C
spearman correlation=-0.3312
ESR1 mRNA expression(log2)
ACSL4 mRNA expression(log2)
D
ACS4 (202422_s_at)
HR = 1.49 (1.17 - 1.9)
logrank P = 0.0012
Probability
Expression
low
high
Time (months)
Number at risk
low 320 82 26 9 2
high 138 25 5 0 0
E
ZFHX1B (203603_s_at)
HR = 1.36 (1.07 - 1.72)
logrank P = 0.01
Probability
Expression
low
high
Time (months)
Number at risk
low 278 73 26 9 2
high 180 34 5 0 0
F
T47D
MCF-7
Taxol-7
MDA-231
BT549
ACSL4
ZEB2
GAPDH
G
patient1
patient2
patient3
patient4
patient5
patient6
patient7
patient8
patient9
ACSL4
ZEB2
GAPDH
H
pearson r = 0.7325
Relative ZEB2 protein expression
Relative ACSL4 protein expression
I
H&E
ACSL4
ZEB2
ER
High ER expression
Low ER expression

Figure2

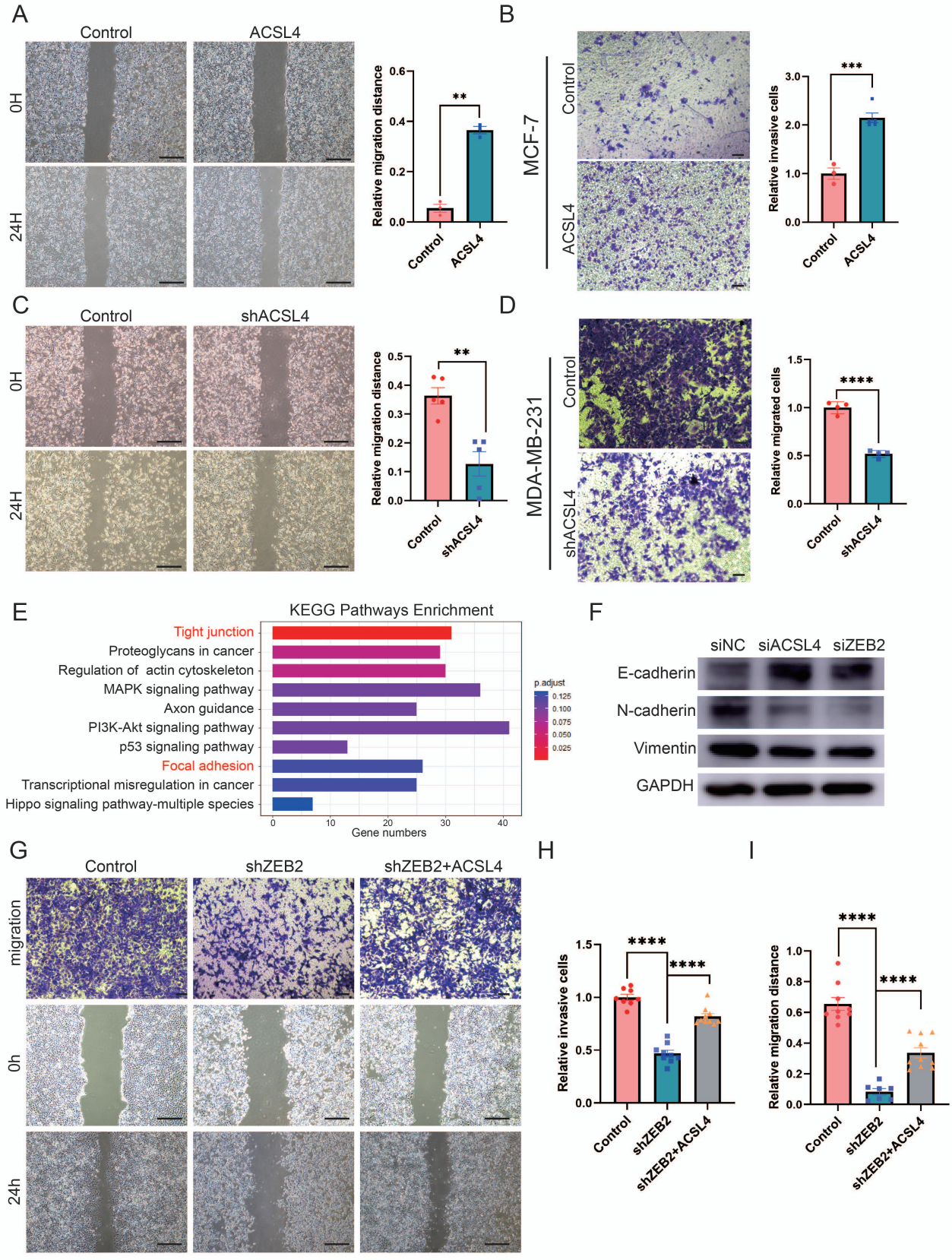
A
Control
ACSL4
0H
24H
Relative migration distance
**
Control
ACSL4
B
MCF-7
Control
ACSL4
Relative invasive cells
***
Control
ACSL4
C
Control
shACSL4
0H
24H
Relative migration distance
**
Control
shACSL4
D
MDA-MB-231
Control
shACSL4
Relative migrated cells
****
Control
shACSL4
E
KEGG Pathways Enrichment
Tight junction
Proteoglycans in cancer
Regulation of actin cytoskeleton
MAPK signaling pathway
Axon guidance
PI3K-Akt signaling pathway
p53 signaling pathway
Focal adhesion
Transcriptional misregulation in cancer
Hippo signaling pathway-multiple species
Gene numbers
p.adjust
F
siNC
siACSL4
siZEB2
E-cadherin
N-cadherin
Vimentin
GAPDH
G
Control
shZEB2
shZEB2+ACSL4
migration
0h
24h
H
Relative invasive cells
****
****
Control
shZEB2
shZEB2+ACSL4
I
Relative migration distance
****
****
Control
shZEB2
shZEB2+ACSL4

Figure 3

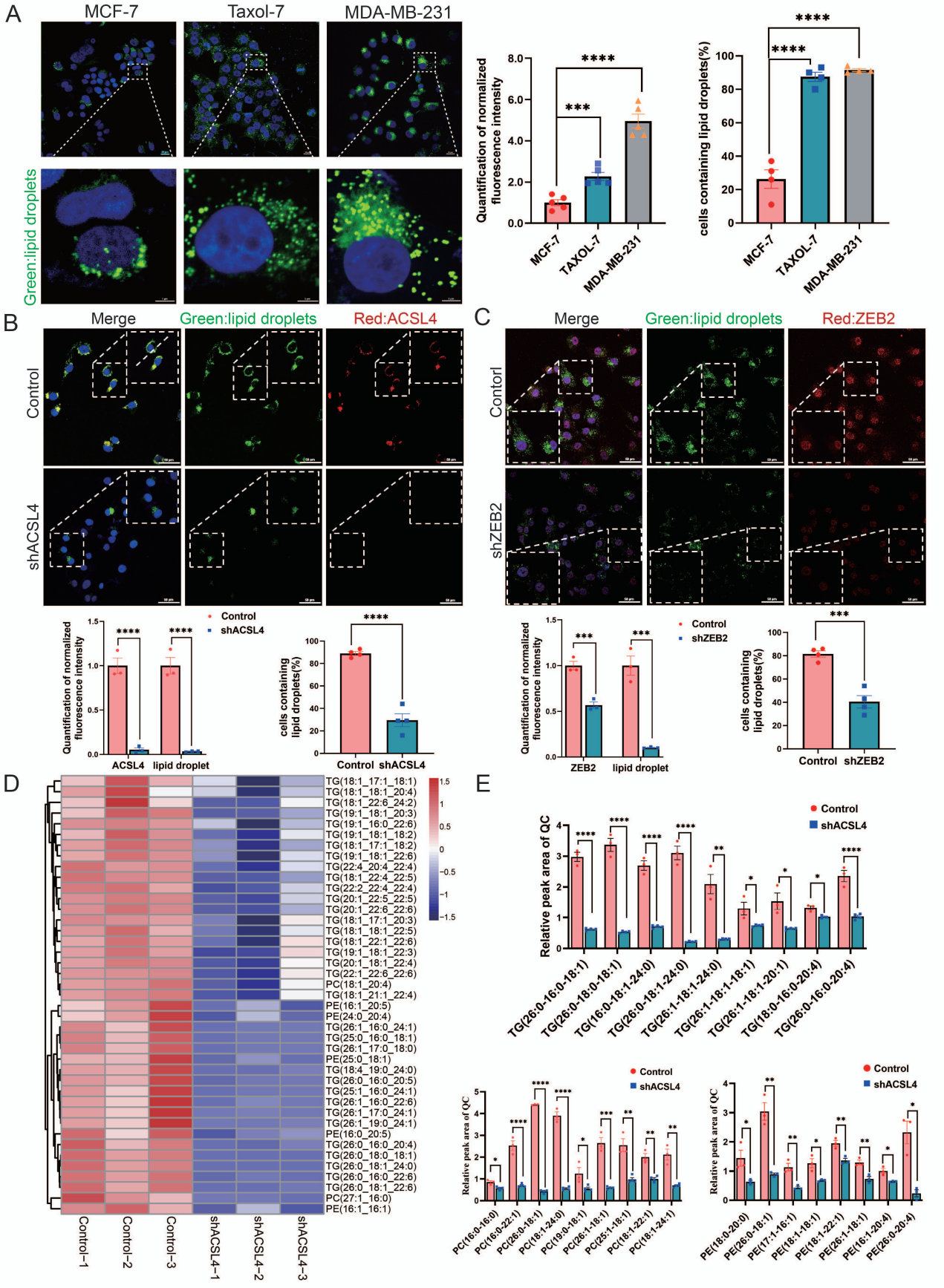
A
MCF-7
Taxol-7
MDA-MB-231
Green:lipid droplets
Quantification of normalized fluorescence intensity
cells containing lipid droplets(%)
MCF-7
TAXOL-7
MDA-MB-231
B
Merge
Green:lipid droplets
Red:ACSL4
Control
shACSL4
ACSL4
lipid droplet
C
Merge
Green:lipid droplets
Red:ZEB2
Contorl
shZEB2
ZEB2
D
Control-1
Control-2
Control-3
shACSL4-1
shACSL4-2
shACSL4-3
E
Relative peak area of QC

Figure4

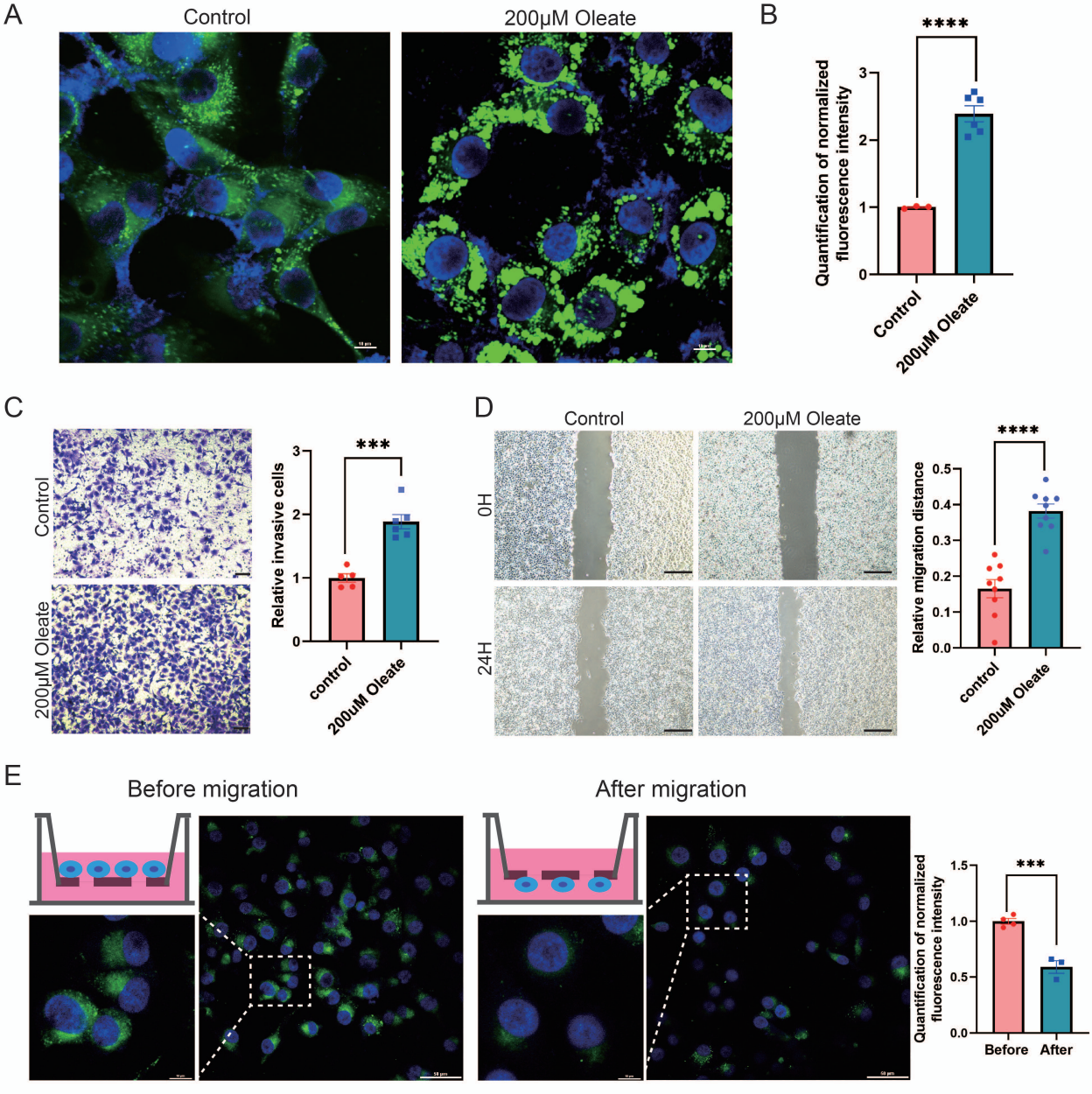
A
Control
200μM Oleate
B
****
Quantification of normalized fluorescence intensity
0
1
2
3
Control
200μM Oleate
C
Control
200μM Oleate
***
Relative invasive cells
0
1
2
3
control
200uM Oleate
D
Control
200μM Oleate
0H
24H
****
Relative migration distance
0.0
0.1
0.2
0.3
0.4
0.5
control
200uM Oleate
E
Before migration
After migration
***
Quantification of normalized fluorescence intensity
0.0
0.5
1.0
1.5
Before
After

Figure 5

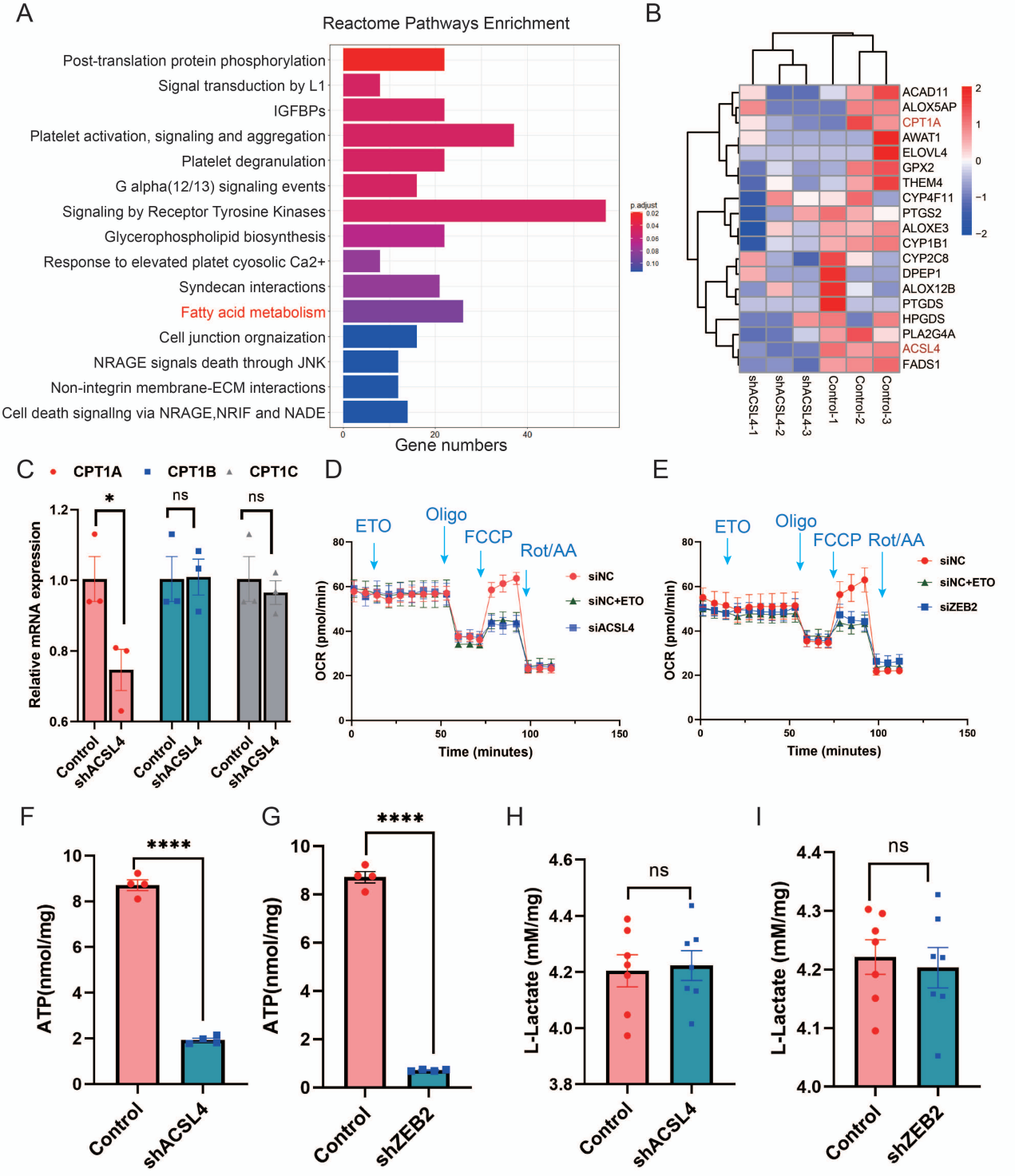
A
Reactome Pathways Enrichment
Post-translation protein phosphorylation
Signal transduction by L1
IGFBPs
Platelet activation, signaling and aggregation
Platelet degranulation
G alpha(12/13) signaling events
Signaling by Receptor Tyrosine Kinases
Glycerophospholipid biosynthesis
Response to elevated platet cyosolic Ca2+
Syndecan interactions
Fatty acid metabolism
Cell junction orgnaization
NRAGE signals death through JNK
Non-integrin membrane-ECM interactions
Cell death signallng via NRAGE,NRIF and NADE
Gene numbers
p.adjust
B
ACAD11
ALOX5AP
CPT1A
AWAT1
ELOVL4
GPX2
THEM4
CYP4F11
PTGS2
ALOXE3
CYP1B1
CYP2C8
DPEP1
ALOX12B
PTGDS
HPGDS
PLA2G4A
ACSL4
FADS1
shACSL4-1
shACSL4-2
shACSL4-3
Control-1
Control-2
Control-3
C
CPT1A
CPT1B
CPT1C
Relative mRNA expression
Control
shACSL4
D
ETO
Oligo
FCCP
Rot/AA
siNC
siNC+ETO
siACSL4
OCR (pmol/min)
Time (minutes)
E
siNC
siNC+ETO
siZEB2
F
ATP(nmol/mg)
Control
shACSL4
G
shZEB2
H
L-Lactate (mM/mg)
I

Figure 6

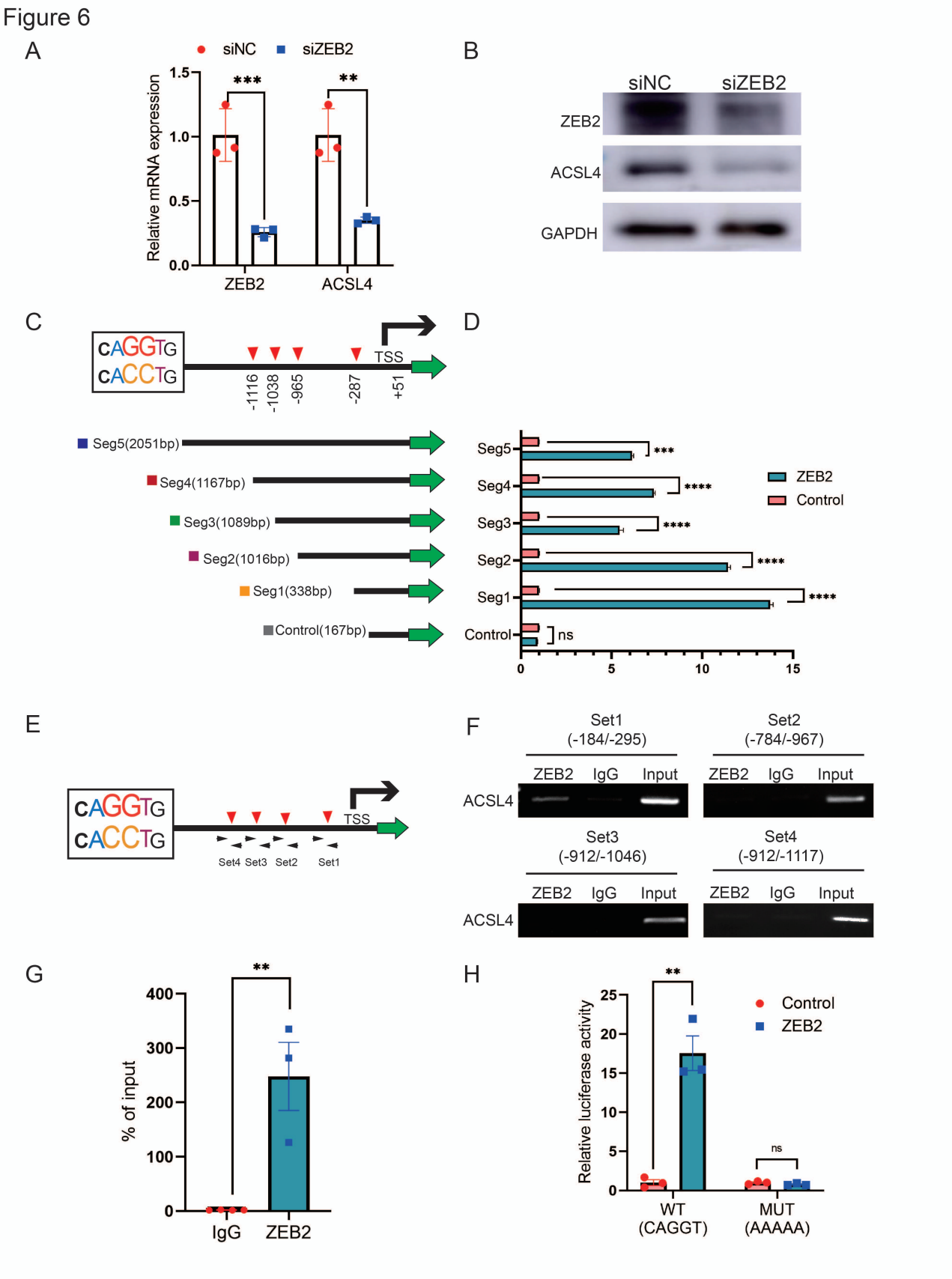
A
siNC
siZEB2
Relative mRNA expression
1.5
1.0
0.5
0.0
***
**
ZEB2
ACSL4
B
siNC
siZEB2
ZEB2
ACSL4
GAPDH
C
cAGGTG
cACCTG
TSS
-1116
-1038
-965
-287
+51
Seg5(2051bp)
Seg4(1167bp)
Seg3(1089bp)
Seg2(1016bp)
Seg1(338bp)
Control(167bp)
D
Seg5
Seg4
Seg3
Seg2
Seg1
Control
ZEB2
Control
***
****
****
****
****
ns
0
5
10
15
E
cAGGTG
cACCTG
TSS
Set4
Set3
Set2
Set1
F
Set1
(-184/-295)
Set2
(-784/-967)
Set3
(-912/-1046)
Set4
(-912/-1117)
ZEB2
IgG
Input
ACSL4
G
**
% of input
400
300
200
100
0
IgG
ZEB2
H
**
Relative luciferase activity
25
20
15
10
5
0
Control
ZEB2
ns
WT
(CAGGT)
MUT
(AAAAA)

Figure 7

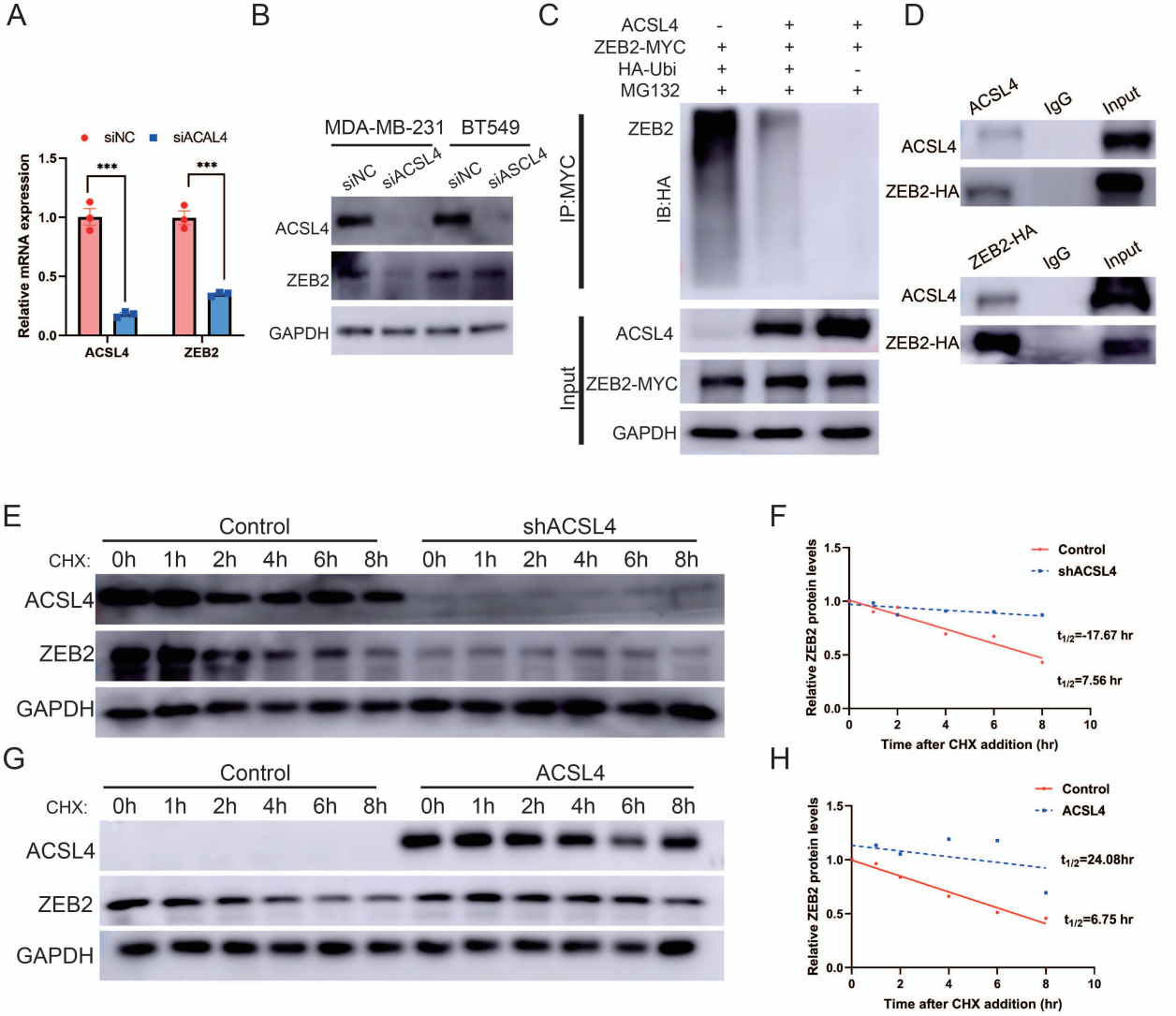
A
siNC
siACAL4
Relative mRNA expression
1.5
1.0
0.5
0.0
***
***
ACSL4
ZEB2
B
MDA-MB-231
BT549
siNC
siACSL4
siNC
siASCL4
ACSL4
ZEB2
GAPDH
C
ACSL4
ZEB2-MYC
HA-Ubi
MG132
IP:MYC
ZEB2
IB:HA
Input
ACSL4
ZEB2-MYC
GAPDH
D
ACSL4
IgG
Input
ACSL4
ZEB2-HA
ZEB2-HA
IgG
Input
ACSL4
ZEB2-HA
E
Control
shACSL4
CHX:
0h
1h
2h
4h
6h
8h
ACSL4
ZEB2
GAPDH
F
Control
shACSL4
Relative ZEB2 protein levels
$t_{1/2}$=-17.67 hr
$t_{1/2}$=7.56 hr
Time after CHX addition (hr)
G
Control
ACSL4
CHX:
ACSL4
ZEB2
GAPDH
H
Control
ACSL4
Relative ZEB2 protein levels
$t_{1/2}$=24.08hr
$t_{1/2}$=6.75 hr
Time after CHX addition (hr)

Figure 8

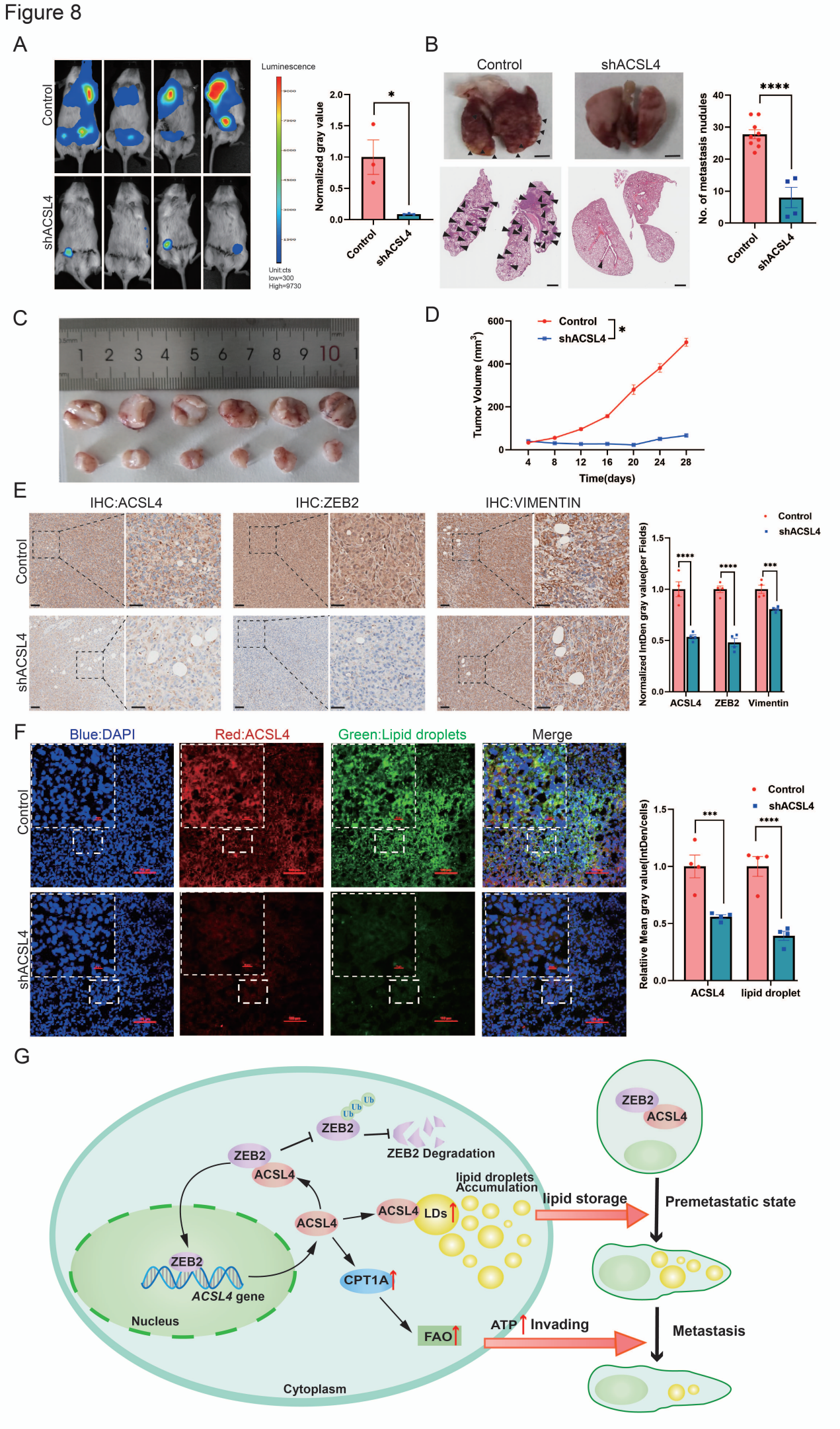
A
Control
shACSL4
Luminescence
Unit:cts
low=300
High=9730
Normalized gray value
Control
shACSL4
B
Control
shACSL4
No. of metastasis nudules
Control
shACSL4
C
D
Control
shACSL4
Tumor Volume (mm3)
Time(days)
E
IHC:ACSL4
IHC:ZEB2
IHC:VIMENTIN
Control
shACSL4
Normalized IntDen gray value(per Fields)
ACSL4
ZEB2
Vimentin
F
Blue:DAPI
Red:ACSL4
Green:Lipid droplets
Merge
Control
shACSL4
Relative Mean gray value(IntDen/cells)
ACSL4
lipid droplet
G
ZEB2
Ub
ZEB2 Degradation
ACSL4
lipid droplets Accumulation
lipid storage
Premetastatic state
LDs
CPT1A
ZEB2
ACSL4 gene
Nucleus
FAO
ATP
Invading
Metastasis
Cytoplasm